IEEE Access
Multidisciplinary | Rapid Review | Open Access Journal

Received March 24, 2021, accepted April 6, 2021, date of publication April 8, 2021, date of current version April 19, 2021.

Digital Object Identifier 10.1109/ACCESS.2021.3071832

Design of Adaptive Fuzzy-Neural-Network-Imitating Sliding-Mode Control for Parallel-Inverter System in Islanded Micro-Grid

YAN YANG[1,2] AND RONG-JONG WAI[1], (Senior Member, IEEE)
[1]Department of Electronic and Computer Engineering, National Taiwan University of Science and Technology, Taipei 106, Taiwan
[2]Faculty of Automation, Huaiyin Institute of Technology, Huai'an 223003, China

Corresponding author: Rong-Jong Wai (rjwai@mail.ntust.edu.tw)

This work was financially supported in part by the Ministry of Science and Technology of Taiwan under Grant MOST 108-2221-E-011-080-MY3, and in part by the Natural Science Research Project of Huaian under Grant HAB201905.

ABSTRACT In this study, an adaptive fuzzy-neural-network-imitating sliding-mode control (AFNNISMC) is developed for a parallel-inverter system in an islanded micro-grid (MG) via a master-slave current sharing strategy. For ensuring the system-level stability, an entire dynamic model is constructed by viewing the parallel-inverter system as a whole. First, a total sliding-mode control (TSMC) scheme, and the TSMC plus an adaptive observer to form an adaptive TSMC (ATSMC) framework are designed for the parallel-inverter system. Then, a four-layer fuzzy neural network (FNN) is investigated to imitate the TSMC law to improve the system robustness, overcome the drawback of the dependence on detailed system dynamics, and deal with the chattering phenomena caused by the TSMC. According to the Lyapunov stability theorem and the projection algorithm, network parameters in the FNN are regulated online by employing the approximation error between the FNN and the TSMC law to ensure the convergence of the network and the stability of the control system. Thereby, the performance of high power quality and high-precision current sharing between inverters can be guaranteed even if system uncertainties exist. Moreover, the proposed AFNNISMC system can achieve the seamless disconnection and re-connection of slave inverters from and into an energized parallel-inverter system, which improves the redundancy and operation flexibility. In addition, numerical simulations and experimental results are given to demonstrate the feasibility and effectiveness of the proposed AFNNISMC scheme. Furthermore, performance comparisons with the ATSMC strategy and a conventional proportional-integral control (PIC) framework are provided to verify the superiority of the proposed scheme.

INDEX TERMS Total sliding-mode control (TSMC), fuzzy neural network (FNN), adaptive control, parallel-inverter system, islanded micro-grid (MG), master-slave current sharing.

I. INTRODUCTION

For the feature of low emissions and high energy efficiency, distributed generation sources (DGs) (e.g., wind generator, photovoltaic, etc.) have attracted great attention as renewable sources [1], [2]. Power inverters are essential to integrate DGs and energy storage systems as a micro-grid (MG), which can connect to the utility grid as well as supply for local loads [3], [4]. With the scale expansion of renewable power generations, the parallel operation of small-scale inverters is used to build a large-capacity MG system by considering switching stresses and system redundancy [5], [6]. Moreover, different DGs are integrated into the point of common coupling (PCC) by their interface inverters to be usually operated in parallel [7].

An islanded MG can provide continuous and reliable power supply for loads, even under the failure of utility grids. In the past, several islanded MG projects had been put into operation for solving the problem of power supply in remote areas and helping to optimize the allocation of power resources [8]. The critical goal of the parallel-inverter system in the islanded MG is to maintain high power quality in the PCC, and improve the dynamic performance and reliability under different load conditions, especially for nonlinear

The associate editor coordinating the review of this manuscript and approving it for publication was Zhilei Yao.

loads. Simultaneously, in order to avoid the over-heating of the electronic devices and delay inverters aging, proportional current/power sharing by the inverter capacity is a vital problem in the parallel-inverter control system [9]. Moreover, system uncertainties in a MG including the fluctuation of the DC voltage, the variation of circuit parameters and external loads, and the system structure alteration caused by disconnection and re-connection of parallel inverters will adversely affect the control performance and system stability. Thus, robust and high-performance control schemes by considering system uncertainties are mandatory to guarantee the robustness of the islanded MG system [10], [11].

The control methods of a parallel-inverter system in an islanded MG can mainly divide into two categories including non-communication-based and communication-based mechanisms. The droop control is a typical non-communication-based strategy, and its flexible plug-and-play function facilitates DGs accessing the MG. However, the voltage control accuracy and power/current sharing are contradictory due to the strong randomness, frequent load variations and nonlinear loads in the MG. Besides, the characteristic of output impedance has a great influence on the control performance, and the additional harmonic droop for nonlinear loads may result in the voltage amplitude drop and oscillation. Various improvement methods are studied in recent years to improve the performance of power quality and current/power sharing. Zhong *et al.* [12] proposed an uncertainty and disturbance estimator (UDE) to estimate and compensate the model non-linearity and system uncertainties in droop controllers to improve the accurate proportional power sharing for inverters in parallel operation. Huang *et al.* [13] presented a decentralized control strategy to achieve both the superior voltage regulation and the power sharing accuracy for a multi-parallel system, and used a coordination control layer to update weight coefficients for realizing the arbitrary power sharing ratio. However, the complexity of the control system increases in [12], [13]. The communication between a parallel-inverter system and a MG central controller (MGCC) was utilized to improve the steady-state and transient performance in [14], [15]. Unfortunately, the communication is always required in [14], [15].

The master-slave control is one of the communication-based strategies in commercial applications especially for remote areas and MGs, because of the superior performance in the power/current sharing and voltage regulation, and insensitivity to line impedance parameters. In the master-slave control method, a voltage controller is usually used in the master inverter to adjust the output voltage and obtain the grid-forming function of a parallel-inverter system, and a local current controller in each slave inverter track the current command provided by the master inverter through a current sharing bus. In view of the rapid development of modern communication technology, some low-cost communication equipment has been adopted for MGs [16]–[19]. Power line communication (PLC) and wireless communication technology have realized the reliable transmission of signals successfully. In general, those model communications reduce the cost greatly, and provide a broader application prospect for the master-slave control method.

In a conventional master-slave control architecture, a proportional-integral control (PIC) is always adopted in the double closed-loop structure for the output voltage and current control in the master inverter, and proportional-integral (PI) current controllers are generally utilized in each slave inverter to track current commands [4]. Although the traditional PIC is simple and easy to realize, the poor tolerance ability to system uncertainties may reduce the control performance due to the existence of system uncertainties in a parallel-inverter system including the DC voltage fluctuation, the external load disturbance, and the structure variation.

To solve the aforementioned problems, Delghavi and Yazdani [11] presented a sliding-mode control (SMC) method by considering an output voltage error and an inductor current error to obtain the high-quality voltage and current protection under external faults. However, if the system uncertainties occur in the reaching phase of the SMC, the designed control system in [11] will lose its robustness. Besides, the prior knowledge of the mathematical model and the corresponding uncertainty bound should be involved in the design, which are difficult to be captured from a practical parallel-inverter system. Tan *et al.* [20] investigated a model-free recursive probabilistic wavelet fuzzy neural network (RPWFNN) for the master inverter to improve the control performance of the output voltage in the master inverter under load variations or external disturbances. Unfortunately, a PI controller was still used for the power regulation in the slave inverter, and the structure uncertainty of a parallel-inverter system was not considered in [20]. Partial inverters will be disconnected from the parallel-inverter system when faults occur, and they will be re-connected after reparation. This will lead to the structure change. From the system modeling viewpoint, the disconnection and re-connection of partial inverters will change the number of poles and zeros of a parallel-inverter system such that the corresponding model-based control systems may be unworkable [21]. On the other hand, the impedance ratio between power sources and practical loads in a parallel-inverter system has a relationship to the number of slave inverter units, which will affect the stability of the whole system. If the number of slave inverter units makes the impedance ratio dissatisfied with the Nyquist stability criterion, the output voltage of the master inverter unit will be unstable [22].

In the previous literatures, the controller is always designed based on the mathematical model of each inverter to meet its stability requirement in a single operation. However, the control performance may be degraded or even unstable in the parallel operation [23] due to the interaction between parallel inverters. It is an effective idea to design a control framework by viewing a parallel-inverter system including a master inverter and n-1 slave inverters as a whole. Moreover, the output voltage of the master inverter and inductance currents of slave inverters are selected as system states

TABLE 1. Research comparisons of different control methods.

Control methods	Main contributions	Potential limitations
Uncertainty and disturbance estimator (UDE)-based robust droop control [12]	✓ Accurate proportional reactive power sharing ✓ Robustness to nonlinear load and system uncertainties	● Dynamic performance to be further improved
Decentralized control strategy [13]	✓ Voltage regulation and proportional power sharing ✓ Improvement on transient performance ✓ Robustness to structure change	● Requirement of low bandwidth communication for proportional power sharing ● Dependence on mathematical model
Droop control combining with a central controller [14]-[15]	✓ Equal power-sharing and voltage amplitude restoration ✓ Improvement on system frequency and phase performance during transient process	● Complex control structure ● Communication-based scheme
Cooperative control combining PI-based master-slave control and droop control [4]	✓ Rapid load sharing response and voltage regulation ✓ Simple controller structure ✓ Steady-state error of nonlinear system	● Poor dynamic performance and robustness ● Communication-based scheme
Robust control-based method with master-slave control [22]	✓ Robustness of system voltage to structure change	● Complexity on weighted-function design
Sliding-mode control with master-slave control [11]	✓ Fast and stable control on voltage and frequency ✓ Protection of power-electronic interface to external faults	● Dependence on mathematical model ● Without robustness to uncertainties in reaching phase of SMC ● Control design to obtain stability of individual inverter
RPWFNN control-based method with master-slave control [20]	✓ Improvement on transient and steady-state responses of voltage control under load variations or external disturbances	● Without considering structure change ● Difficult to tune PI control gains in slave inverter

and the parallel-inverter control is considered as a comprehensive problem to achieve the control goal and system stability. The major contributions and potential limitations of the previous researches in [4], [11]–[15], [20] and [22] are summarized in Table 1. The motivation of this study is to design a model-free control strategy for the parallel-inverter system with a master-slave current sharing scheme in an islanded MG, realize the accurate voltage tracking and current sharing both under the occurrence of parameter variations and structure uncertainties, and ensuring the system-level stability with global robustness.

A total sliding-mode control (TSMC) is an effective method to deal with system uncertainties and has global robustness without the reaching phase in the conventional SMC. As for a parallel-inverter system, each state error is always used to construct an element of the sliding-surface vector, which generates the control effort of each inverter. However, it is hard to capture accurate bounds of system uncertainties in an actual parallel-inverter system, which makes the desired control performance difficult to achieve. Besides, the chatting phenomenon is an inherent defection due to the utilization of a sign function with a large coefficient to cope with dynamics caused by system uncertainties. Li *et al* [24] designed an adaptive SMC scheme to estimate bounds of nonlinear terms and external disturbances online to reduce the chattering phenomena for a Markov jump nonlinear system. But the dependence on the prior knowledge of system parameters remains unresolved.

By considering system uncertainties, an intelligent-based estimator could be an alternative scheme with merits of self-learning, capability of approximating any unknown smooth functions, and relief from system models. Zhong *et al.* [25] developed an adaptive fuzzy algorithm for a friction compensator by combining the TSMC to improve the robust ability of a multi-axis motion system. Haq *et al.* [26] designed a neural network (NN) to estimate uncertainties for a global SMC framework to suppress the chattering phenomena in a variable-speed wind-turbine control system.

In recent years, various machine learning (ML) algorithms have received more attention, especially for the data science community. ML models, which are usually expected to learn from big data, can be used to inform future decisions for prediction and classification. In general, the model training and operation of ML are carried out off line on computers, which require a high processing power. A NN is essentially a part of deep learning, which in turn is a subset of ML. The mathematical representation of the NN is helpful for combining the system dynamic model to prove the system stability, and the on-line learning ability of the NN is more suitable for real-time control applications than other ML algorithms. In the last few decades, the concept of incorporating fuzzy logic into a NN has been grown into a popular research topic [27]. In contrast to a pure NN or a fuzzy system, a fuzzy neural network (FNN) possesses both their advantages. The FNN combines the capability of fuzzy reasoning in handling uncertain information and the capability of artificial neural networks in learning from process [28]. It has been proven that the FNN can approximate a wide range of nonlinear functions to any desired degree of accuracy under certain condition [29]. Chu *et al.* [29] adopted a double hidden-layer feedback NN to approach the unknown part in the designed controller for an active power filter (APF), and improved the response

characteristic and power quality under parameter variations and external disturbances. Hou and Fei [30] developed a meta-cognitive FNN (MCFNN) framework to estimate the uncertain term for the global sliding-mode control (GSMC) law, and the control performance was verified on an APF. Moreover, a recurrent feature selection neural network (RFSNN) was proposed to mimic the uncertain compensation current in an APF system in [31]. The RFSNN in [31] combining with the GSMC can reduce the computational burden of NN with full parameters adjustment and assure a high-performance current control. An adaptive type-2 FNN control system with an uncertainty compensator was proposed to enhance the ability representing system uncertainties and the performance of power quality improvement for an APF in [32]. However, intelligent strategies in [28]–[31] just work as auxiliary controllers to approximate unknown functions or estimate system uncertainties for improving the control performance, and an extra compensation controller is required in [32]. As a result, the complexity of the whole control system will be increased.

A FNN-based control method has the learning and reasoning ability due to the combination of fuzzy logic and NN. In [20], the output voltage errors and their changes were taken as inputs for a FNN to obtain the robustness of the output voltage to load variations. However, in high-order or multi-state systems, the number of fuzzy rules (i.e., the FNN size) is an important issue that has to be faced. Integrating the SMC technique with the FNN can significantly reduce the network size. In this study, an adaptive fuzzy-neural-network-imitating sliding-mode control (AFNNISMC) scheme is developed by considering the non-linearity and uncertainties of a parallel-inverter system in an islanded MG. For ensuring the system-level stability, the parallel-inverter system with a master inverter and n-1 slave inverters is considered as a whole. Moreover, the output voltage and filter inductor currents are selected as system states to establish a total sliding-surface vector. In addition, a FNN is taken as the main controller to imitate the TSMC without the requirement of an auxiliary controller. The elements in sliding-surface vector are selected as the input signals for the FNN to reduce the network size, and network parameters in the FNN are trained online to improve the voltage tracking and current sharing precision even in the presence of system uncertainties. Furthermore, the network structure is unnecessary to change with the disconnection and re-connection of partial slave inverters. The proposed model-free AFNNISMC scheme can effectively improve the robustness of the parallel-inverter system against system uncertainties. The major contributions of this study are summarized as follows: 1) The entire dynamic model of a parallel-inverter system in an islanded MG is constructed by viewing this parallel-inverter system with a master inverter and other n-1 slave inverters as a whole to obtain the system-level design. 2) The proposed AFNNISMC framework with online learning mechanisms has robustness against system uncertainties for relaxing the requirement of detailed system dynamics, and alleviating the chattering phenomena in the voltage tracking and current sharing. 3) The FNN structure in the proposed AFNNISMC system is unnecessary to change when the connection structure of parallel inverters is varied, so that one can guarantee robustness against parameter variations and structure uncertainties. Moreover, the proposed AFNNISMC system enhances the scalability, redundancy, and operational flexibility of slave inverters.

Following the introduction, system descriptions and dynamic models of a parallel-inverter system in an islanded MG are introduced in Section II. The detail design process of the designed ATMSC and the proposed AFNNISMC for the voltage tracking and current sharing are investigated in Section III and IV, respectively. The feasibility and effectiveness of the proposed AFNNISMC framework are demonstrated by numerical simulations and experimental verifications in Section V. Finally, Section VI draws some conclusions of this study.

II. SYSTEM DESCRIPTIONS

A parallel-inverter system is connected to a common AC load including n single-phase PWM full-bridge inverters in an islanded micro-grid (MG) as shown in Fig. 1. This parallel-inverter system consists of a master inverter and n-1 slave inverters. The master inverter is equipped with four power switches (T_{A1+}, T_{A1-}, T_{B1+}, T_{B1-}) and an LC low-pass filter composed by an inductor (L_{f1}) and a capacitor (C_{f1}). The n-1 slave inverters have the same circuit structure as the master inverter. All inverters are connected in

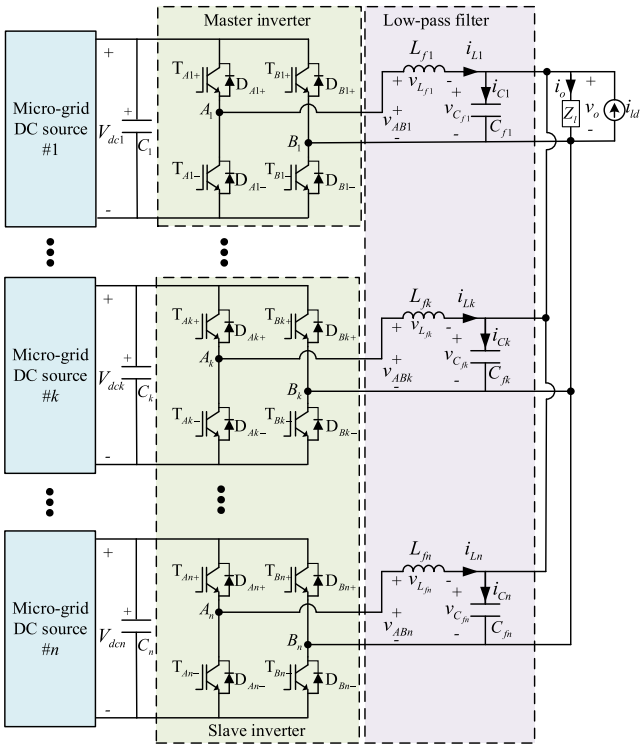

FIGURE 1. Framework of parallel-inverter system in islanded micro-grid under master-slave current sharing strategy.

parallel to a common connection point, and supply power for an equivalent load (Z_l).

In Fig. 1, V_{dc1}, V_{AB1}, v_{Lf1} and v_{Cf1} are the voltages of DC bus, the inverter, the filter inductor, and the filter capacitor in the master inverter terminal, respectively; V_{dck}, v_{ABk}, v_{Lfk} and v_{Cfk} are the corresponding voltages of the slave inverter, and the subscript k ($k = 2, \cdots, n$) indicates the kth inverter. i_{L1} and i_{C1} are the inductor and capacitor currents in the master inverter, respectively; $i_{Lk}|_{k=2,\cdots,n}$ and $i_{Ck}|_{k=2,\cdots,n}$ are the corresponding inductor and capacitor currents in the kth inverter. i_o and v_o denote the output current and voltage of the parallel-inverter system for the load. The external disturbance incurred by load variations or unpredictable uncertainties is emulated by the current source (i_{ld}).

By viewing the parallel-inverter system with a master inverter and n-1 slave inverters as a whole, the mathematical model of the parallel-inverter system in Fig. 1 can be derived. In this derivation, the equivalent resistors of inductors and capacitors are small enough to be ignored. According to the Kirchhoff current law (KCL) in the node of the load (Z_l), one can obtain

$$i_{L1} + \sum_{k=2}^{n} i_{Lk} - \sum_{k=1}^{n} i_{Ck} - i_o + i_{ld} = 0 \tag{1}$$

Because the relationship of voltages and currents in filter capacitors can be expressed as $i_{Ck} = C_{fk}\dot{v}_{Cfk}\big|_{k=1,\cdots,n}$, and the capacitors in each module are parallel to the load (Z_l), the capacitor voltage equals the output voltage ($v_{Cfk}\big|_{k=1,\cdots,n} = v_o$), and $\sum_{k=1}^{n} i_{Ck} = (\sum_{k=1}^{n} C_{fk})\dot{v}_o = C\dot{v}_o$, in which $C = \sum_{k=1}^{n} C_{fk}$ is the summation of filter capacitors in each module.

According to the Kirchhoff voltage law (KVL) in the filter loop of each inverter, it can yield

$$\dot{i}_{L1} = \frac{1}{L_{f1}}(D_1 V_{dc1} - v_{Cf1}) \tag{2a}$$

$$\dot{i}_{Lk} = (D_k V_{dck} - v_{Cfk})/L_{fk}\big|_{k=2,\cdots,n} \tag{2b}$$

where D_1 and D_k are the duty cycles of the power switches in the master inverter and other n-1 slave inverters under the unipolar sinusoidal pulse-width-modulation (SPWM), respectively. By defining a sinusoidal control signal (v_{con1}) as the modulation signal of the master inverter and selecting a triangular wave with the amplitude of $\hat{v}_{tri}$ as the carrier signal, the duty cycle of the master inverter can be expressed as $D_1 = v_{con1}/\hat{v}_{tri}$, and the corresponding power gain of the master inverter can be represented as $K_{\mathrm{PWM1}} = V_{dc1}/\hat{v}_{tri}$. By using the aforementioned definitions to n-1 slave inverters, the representations of $D_{k,}$, v_{conk}, and $K_{\mathrm{PWM}k}$ with the subscript k ($k = 2, \cdots, n$) can be obtained, respectively. By substituting (2a) to the time derivative of (1), the dynamic model of the parallel-inverter system in an islanded MG can be represented as

$$\begin{bmatrix} \ddot{v}_o \\ \dot{i}_{L2} \\ \vdots \\ \dot{i}_{Ln} \end{bmatrix} = \begin{bmatrix} -1/CL_{f1} & 0 \cdots 0 \\ -1/L_{f2} & 0 \cdots 0 \\ \vdots & \vdots \quad \vdots \\ -1/L_{fn} & 0 \cdots 0 \end{bmatrix} \begin{bmatrix} v_o \\ i_{L2} \\ \vdots \\ i_{Ln} \end{bmatrix} + \mathrm{diag}\left(\frac{K_{\mathrm{PWM1}}}{CL_{f1}}, \frac{K_{\mathrm{PWM2}}}{L_{f2}}, \cdots, \frac{K_{\mathrm{PWM}n}}{L_{fn}}\right) \begin{bmatrix} v_{con1} \\ v_{con2} \\ \vdots \\ v_{conn} \end{bmatrix} + \begin{bmatrix} 1/C & 0 \cdots 0 \\ 0 & 0 \cdots 0 \\ \vdots & \vdots \quad \vdots \\ 0 & 0 \cdots 0 \end{bmatrix} \begin{bmatrix} z_1 \\ 0 \\ \vdots \\ 0 \end{bmatrix} + \begin{bmatrix} \phi \\ 0 \\ \vdots \\ 0 \end{bmatrix} \tag{3}$$

where $z_1 = (\sum_{k=2}^{n} \dot{i}_{Lk}) - \dot{i}_o$; $\phi = i_{ld}/C$; diag(·) denotes a $n \times n$ diagonal matrix, in which the numbers in parentheses are the elements on the diagonal of the diagonal matrix.

As for the master-slave current sharing scheme, the master inverter works as the voltage source to regulate the output voltage and provide the reference current signal. Moreover, n-1 slave inverters act as current sources to track the corresponding reference currents. The output voltage (v_o) and the inductor currents of slave inverters ($i_{Lk}|_{k=2,\cdots,n}$) are selected as system states; v_{con1} and $v_{conk}|_{k=2,\cdots,n}$ are control efforts to be designed later for the master and slave inverters.

In practical applications, system parameters are hard to precisely obtain. Besides, the fluctuation of the DC voltage caused by distributed generation systems (DGs), and the disturbance of load variations also should be considered.

Because the coefficients in (3) can be divided into the nominal part and the uncertain part, the dynamic model of the parallel-inverter system can be rewritten as

$$\begin{aligned} \begin{bmatrix} \ddot{x}_1 \\ \dot{x}_2 \\ \vdots \\ \dot{x}_n \end{bmatrix} &= \mathbf{A}_p \boldsymbol{x} + \mathbf{B}_P \boldsymbol{u} + \mathbf{C}_p z + \boldsymbol{\varphi} \\ &= (\mathbf{A}_{pn} + \Delta\mathbf{A}_{pn})\boldsymbol{x} + (\mathbf{B}_{pn} + \Delta\mathbf{B}_{pn})\boldsymbol{u} \\ &\quad + (\mathbf{C}_{pn} + \Delta\mathbf{C}_{pn})z + \boldsymbol{\varphi} \\ &= \mathbf{A}_{pn}\boldsymbol{x} + \mathbf{B}_{Pn}\boldsymbol{u} + \mathbf{C}_{pn} z + \boldsymbol{\psi} \end{aligned} \tag{4}$$

where $\boldsymbol{x} = [v_o, \ i_{L2}, \cdots, i_{Ln}]^T \in \boldsymbol{R}^{n\times 1}$; $\boldsymbol{u}$=$[v_{con1}, v_{con2}, \cdots, v_{conn}]^T \in \boldsymbol{R}^{n\times 1}$; $z = [z_1, 0, \cdot\cdot, 0]^T \in \boldsymbol{R}^{n\times 1}$; $\varphi = [\phi, 0 \cdot 0]^T \in \boldsymbol{R}^{n\times 1}$;

$$\mathbf{A}_p = \begin{bmatrix} a_{p1} & 0 \cdots 0 \\ a_{p2} & 0 \cdots 0 \\ \vdots & \vdots \quad \vdots \\ a_{pn} & 0 \cdots 0 \end{bmatrix} \in \boldsymbol{R}^{n\times n}$$

with $a_{p1} = -1/(L_{f1}C)$, $a_{p2} = -1/L_{f2}$, and $a_{pn} = -1/L_{fn}$, in which the nominal matrix of $\boldsymbol{A}_p$ can be represented as

$$\mathbf{A}_{pn} = \begin{bmatrix} a_{pn1} & 0 \cdots 0 \\ a_{pn2} & 0 \cdots 0 \\ \vdots & \vdots \quad \vdots \\ a_{pnn} & 0 \cdots 0 \end{bmatrix} \in \boldsymbol{R}^{n\times n},$$

and its uncertain matrix can be expressed as

$$\Delta\mathbf{A}_p = \begin{bmatrix} \Delta a_{p1} 0 \cdots 0 \\ \Delta a_{p2} 0 \cdots 0 \\ \vdots\vdots \\ \Delta a_{pn} 0 \cdots 0 \end{bmatrix} \in \boldsymbol{R}^{n\times n};$$

$$\mathbf{B}_p = \text{diag}(b_{p1}, b_{p2}, \cdots, b_{pn}) \in \boldsymbol{R}^{n\times n}$$

with $b_{p1} = K_{\text{PWM1}}/(L_{f1}C)$, $b_{p2} = K_{\text{PWM2}}/L_{f2}$, and $b_{pn} = K_{\text{PWM}n}/L_{fn}$, in which the nominal matrix of $\boldsymbol{B}_p$ can be represented as $\mathbf{B}_{pn} = \text{diag}(b_{pn1}, b_{pn2}, \cdots, b_{pnn}) \in \boldsymbol{R}^{n\times n}$, and its uncertain matrix can be expressed as $\Delta\mathbf{B}_p = \text{diag}(\Delta b_{p1}, \Delta b_{p2}, \cdots, \Delta b_{pn}) \in \boldsymbol{R}^{n\times n}$;

$$\mathbf{C}_p = \begin{bmatrix} c_p & 0 \cdots 0 \\ 0 & 0 \cdots 0 \\ \vdots & \vdots \quad \vdots \\ 0 & 0 \cdots 0 \end{bmatrix} \in \boldsymbol{R}^{n\times n}$$

with $c_p = 1/C$, in which the nominal matrix of $\boldsymbol{C}_p$ can be represented as

$$\mathbf{C}_{pn} = \begin{bmatrix} c_{pn} & 0 \cdots 0 \\ 0 & 0 \cdots 0 \\ \vdots & \vdots \quad \vdots \\ 0 & 0 \cdots 0 \end{bmatrix} \in \boldsymbol{R}^{n\times n},$$

and its uncertain matrix can be expressed as

$$\Delta\mathbf{C}_p = \begin{bmatrix} \Delta c_p & 0 \cdots 0 \\ 0 & 0 \cdots 0 \\ \vdots & \vdots \quad \vdots \\ 0 & 0 \cdots 0 \end{bmatrix} \in \boldsymbol{R}^{n\times n};$$

$a_{pn1}, b_{pn1}, a_{pn2}, b_{pn2}, a_{pnn}, b_{pnn}$ and c_{pn} represent the nominal values of a_{p1}, b_{p1}, a_{p2}, b_{p2}, a_{pn}, b_{pn} and c_p, respectively; $\Delta a_{p1}, \Delta b_{p1}, \Delta a_{p2}, \Delta b_{p2}, \Delta a_{pn}, \Delta b_{pn}$ and Δc_p denote the difference between real and nominal values. In (4), the lumped uncertainty vector in the parallel-inverter system can be defined as

$$\boldsymbol{\psi} = \Delta\boldsymbol{A}_{pn}\boldsymbol{x} + \Delta\mathbf{B}_{pn}\boldsymbol{u} + \Delta\boldsymbol{C}_{pn}\boldsymbol{z} + \boldsymbol{\varphi} \tag{5}$$

Assumption 1: The boundary value of the lumped uncertainty vector is assumed as

$$\|\boldsymbol{\psi}\|_1 < \rho \tag{6}$$

where $\|\cdot\|_1$ denotes the 1-norm operator, and ρ is a given positive constant.

As for a real circuit, the deviations of filter inductors (L_{f1} and $L_{fk}|_{k=2,\cdots,n}$) and filter capacitors (C_{f1} and $C_{fk}|_{k=2,\cdots,n}$) are limited to be about $\pm 10\%$, and their corresponding internal equivalent resistances are small enough to be neglected. Moreover, the output control effort vector ($\boldsymbol{u}$) is always limited by hardware digital/analog (D/A) ports, even for the divergence of the control law. For practical applications, the time derivative term $(\Delta c_p[(\sum_{k=2}^{n} \dot{i}_{Lk}) - \dot{i}_o])$ is derived in a discrete form $(\Delta c_p[(\sum_{k=2}^{n} \frac{i_{Lk}(j) - i_{Lk}(j-1)}{T_s}) - \frac{i_o(j) - i_o(j-1)}{T_s}])$, where j is the sampling instant, and T_s is the sampling period. The sampling period (T_s) is not infinitesimal, e.g., it is equal to 0.05ms due to the sampling frequency of 20kHz. Therefore, the time derivative term $(\Delta c_p[(\sum_{k=2}^{n} \dot{i}_{Lk}) - \dot{i}_o])$ is bounded. In addition, the current source (i_{ld}) for representing unpredictable uncertainties in a real worktable system also will be bounded. Thus, the lumped uncertainty vector in (5) can be reasonably assumed to be bounded by a positive constant for a real system.

An appropriate control effort ($\boldsymbol{u}$) will be designed to force the state vector ($\boldsymbol{x}$) to track the reference vector ($\boldsymbol{x}^{ref} = [v_o^{ref}, i_{L2}^{ref}, \cdots, i_{Ln}^{ref}]$), where v_o^{ref} is the reference voltage, and the reference current is set as $i_{Lk}^{ref} = p_k \cdot i_{L1}\big|_{k=2,\cdots,n}$, in which $0 < p_k \leq 1$ represents the proportional coefficient of the reference current for the kth inverter by considering the inverter capacities to perform the proportional current sharing.

III. ATSMC DESIGN

In this section, a total sliding-mode control (TSMC) scheme, and the TSMC plus an adaptive observer to form an adaptive TSMC (ATSMC) framework for a parallel-inverter system in an islanded micro-grid (MG) with the master-slave current sharing scheme is depicted in Fig. 2(a). The TSMC scheme comprises the baseline model design and the curbing controller design. Firstly, the baseline model design ($\boldsymbol{u}_b$) is given based on the nominal model to specify the desired performance. Moreover, to enhance the robustness to the unpredictable disturbance, the curbing controller design ($\boldsymbol{u}_c$) is addressed to assure the performance of the baseline model design. In addition, an adaptive observer is introduced into the TSMC scheme to form the ATSMC framework for estimating the bound of the lumped uncertainty vector to relieve the chattering phenomena in the TSMC system.

By selecting the output voltage (v_o) and the inductor currents ($i_{Lk}|_{k=2,\cdots,n}$) of slave inverters as system states, a TSMC system is designed for the parallel-inverter system to obtain the high-quality output voltage and realize the current sharing control under the existence of system uncertainties. First, the voltage tracking and current sharing errors are defined as

$$e_v = v_o^{ref} - v_o \tag{7a}$$

$$e_{ik} = i_{Lk}^{ref} - i_{Lk}\big|_{k=2,\cdots,n} \tag{7b}$$

Then, a total sliding-surface vector is designed as follows:

$$\boldsymbol{s}(t) = [s_v\ s_{i2}\ \cdots\ s_{in}]^T = f(\boldsymbol{e}) - f(\boldsymbol{e}_0) + \int_0^t \frac{\partial f}{\partial \boldsymbol{e}^T}\mathbf{J}\boldsymbol{e}d\tau \tag{8}$$

where $\boldsymbol{e} = [\dot{e}_v, e_v, e_{i2}, \cdots, e_{in}]^T \in \boldsymbol{R}^{(n+1)\times 1}$; $\boldsymbol{e}_0$ is the initial value of $\boldsymbol{e}(t)$; $\boldsymbol{s}(0) = \boldsymbol{0} \in \boldsymbol{R}^{n\times 1}$; $\mathbf{J} = \text{diag}(\mathbf{J}_v, \mathbf{J}_i) \in \boldsymbol{R}^{(n+1)\times(n+1)}$ with

$$\mathbf{J}_v = \begin{bmatrix} k_{v1} & k_{v2} \\ 1 & 0 \end{bmatrix} \in \boldsymbol{R}^{2\times 2}$$

and $\mathbf{J}_i = \text{diag}(k_{i2}, \cdots, k_{in}) \in \boldsymbol{R}^{(n-1)\times(n-1)}$, in which k_{v1}, k_{v2}, and $k_{ik}|_{k=2,\cdots,n}$ are positive constants;

$$\frac{\partial f}{\partial e^T} = \begin{bmatrix} b_{pn1}^{-1} & 0 & 0 & \cdots & 0 \\ 0 & 0 & b_{pn2}^{-1} & \cdots & 0 \\ \vdots & \vdots & \vdots & \ddots & \vdots \\ 0 & 0 & 0 & \cdots & b_{pnn}^{-1} \end{bmatrix} \in \boldsymbol{R}^{n\times(n+1)}.$$

By taking the differential of (8) with respect to time, one can obtain

$$\dot{\boldsymbol{s}}(t) = \frac{\partial f}{\partial \boldsymbol{e}^T}\dot{\boldsymbol{e}} + \frac{\partial f}{\partial \boldsymbol{e}^T}\mathbf{J}\boldsymbol{e} = 0 \tag{9}$$

Theorem 1: If the parallel-inverter system shown in (4) is controlled by the TSMC law described in (10), the objective of the voltage tracking and the current sharing can be achieved, and the system stability can be ensured even in the presence of system uncertainties.

$$\boldsymbol{u}_{\text{TSMC}} = \boldsymbol{u}_b + \boldsymbol{u}_c \tag{10a}$$

$$u_b = -\mathbf{B}_{pn}^{-1}(\boldsymbol{A}_{pn}x + \boldsymbol{C}_{pn}z - \dot{x}^{ref}) + \frac{\partial f}{\partial e^T}Je \tag{10b}$$

$$\boldsymbol{u}_c = \mathbf{B}_{pn}^{-1}[\rho\,\text{sgn}(\boldsymbol{s}) + K_s\boldsymbol{s}] \tag{10c}$$

where $\boldsymbol{u}_{\text{TSMC}} = [u_{\text{TSMC1}}, u_{\text{TSMC2}}, \cdots, u_{\text{TSMCn}}]^T \in \boldsymbol{R}^{n\times 1}$; ρ is the gain of the curbing control law to be designed later; sgn$(\cdot)$ is the sign function operator, $\mathbf{K_s}$= diag$(k_{s1}, k_{s2}, \cdots, k_{sn}) \in \boldsymbol{R}^{n\times n}$.

Proof: By defining the first Lyapunov function candidate $V_s = \boldsymbol{s}^T\boldsymbol{s}/2$, one can obtain its derivative as

$$\begin{aligned}\dot{V}_s &= \boldsymbol{s}^T\dot{\boldsymbol{s}} = \boldsymbol{s}^T\mathbf{B}_{pn}^{-1}[-\rho\,\text{sgn}(\boldsymbol{s}) - \mathbf{K}_s\boldsymbol{s} + \boldsymbol{\psi}] \\ &\le -\boldsymbol{s}^T\mathbf{B}_{pn}^{-1}\mathbf{K}_s\boldsymbol{s} - \left\|\boldsymbol{s}^T\mathbf{B}_{pn}^{-1}\right\|_1(\rho - \|\boldsymbol{\psi}\|_1)\end{aligned} \tag{11}$$

As long as the condition of $\rho > \|\boldsymbol{\psi}\|_1$ holds, (11) can be rewritten as

$$\dot{V}_s \le -\boldsymbol{s}^T\mathbf{B}_{pn}^{-1}\mathbf{K}_s\boldsymbol{s} \le 0 \tag{12}$$

From (11) and (12), it is obvious that the first Lyapunov function $V_s > 0$ and its derivative $\dot{V}_s \le 0$, which means that the TSMC system can be guaranteed to be stable. This finishes the proof of Theorem 1. However, the chatting phenomena will be inevitable due to the conservative selection of a large value for the control gain (ρ) to cope with system uncertainties.

Generally speaking, the issue of chattering with oscillations of finite amplitude and very high frequency to be appeared in the control input has a detrimental effect on the life of the control actuator. Fortunately, the term of $\mathbf{B}_{pn}^{-1}\mathbf{K}_s\boldsymbol{s}$ introduced into the curbing control law (10c) is helpful to reduce the chattering phenomena caused by the sign function. It is because the increasing of the gain matrix ($\mathbf{K}_s$) properly can dominate the fact that $\dot{V}_s \le -\boldsymbol{s}^T\mathbf{B}_{pn}^{-1}\mathbf{K}_s\boldsymbol{s} \le 0$, even the worst case $\rho < \|\boldsymbol{\psi}\|_1$ happens. Therefore, the upper bound (ρ) of the lumped uncertainty vector could be conservatively selected to avoid the increasing of the chattering phenomena caused by the sign term $\mathbf{B}_{pn}^{-1}\rho sgn(\boldsymbol{s})$ in (10c).

Theorem 2: If the curbing controller ($\boldsymbol{u}_c$) in (10a) is replaced by $\boldsymbol{u}_{ca}$ in (13a) with an adaptive observer for the bound of the system uncertainty vector designed in (13b), the stability of the designed ATSMC system with the control law $\boldsymbol{u}_{\text{ATSMC}} = \boldsymbol{u}_b + \boldsymbol{u}_{ca}$ for the parallel-inverter system with the master-slave current sharing control scheme can be guaranteed.

$$\boldsymbol{u}_{ca} = \mathbf{B}_{pn}^{-1}[\hat{\rho}\,\text{sgn}(\boldsymbol{s}) + \mathbf{K}_s\boldsymbol{s}] \tag{13a}$$

$$\dot{\hat{\rho}}(t) = \frac{1}{\lambda}\left\|\boldsymbol{s}^T\mathbf{B}_{pn}^{-1}\right\|_1 \tag{13b}$$

where $\hat{\rho}$ is the estimated value of ρ in (10c); λ is an adaptive learning rate.

Proof: By defining an estimated error as $\tilde{\rho} = \rho - \hat{\rho}$, and the second Lyapunov function as $V_{sa} = \boldsymbol{s}^T\boldsymbol{s}/2 + \lambda\tilde{\rho}^2/2$, one can obtain its derivative as

$$\begin{aligned}\dot{V}_{sa} &= \boldsymbol{s}^T\dot{\boldsymbol{s}} + \lambda\tilde{\rho}\dot{\tilde{\rho}} \\ &= \boldsymbol{s}^T\mathbf{B}_{pn}^{-1}[-\hat{\rho}\,\text{sgn}(\boldsymbol{s}) - \mathbf{K}_s\boldsymbol{s} - \boldsymbol{\psi}] - \lambda(\rho - \hat{\rho})\dot{\hat{\rho}} \\ &\le -\boldsymbol{s}^T\mathbf{B}_{pn}^{-1}\mathbf{K}_s\boldsymbol{s} - \hat{\rho}\left\|\boldsymbol{s}^T\mathbf{B}_{pn}^{-1}\right\|_1 - \boldsymbol{s}^T\mathbf{B}_{pn}^{-1}\boldsymbol{\psi} + \lambda\hat{\rho}\dot{\hat{\rho}} - \lambda\rho\dot{\hat{\rho}} \\ &\le -\boldsymbol{s}^T\mathbf{B}_{pn}^{-1}\mathbf{K}_s\boldsymbol{s} - \left\|\boldsymbol{s}^T\mathbf{B}_{pn}^{-1}\right\|_1(\rho - \|\boldsymbol{\psi}\|_1)\end{aligned} \tag{14}$$

As long as the condition of $\rho > \|\boldsymbol{\psi}\|_1$ holds, (14) can be rewritten as

$$\dot{V}_{sa} \le -\boldsymbol{s}^T\mathbf{B}_{pn}^{-1}\mathbf{K}_s\boldsymbol{s} \le 0 \tag{15}$$

From (14) and (15), the second Lyapunov function for the ATSMC system $V_{sa} > 0$ and its derivative $\dot{V}_{sa} \le 0$. Because the result of $V_{sa}(\boldsymbol{s}(t), \tilde{\rho}(t)) \le V_{sa}(\boldsymbol{s}(0), \rho(0))$ can be satisfied, it means that $\boldsymbol{s}(t)$ and $\tilde{\rho}(t)$ are bounded functions. According to the Lyapunov stability theory and the Barbalat's lemma [33], it can conclude that the sliding-surface vector $\boldsymbol{s}(t)$ will converge to zero as $t \to \infty$. Thus, the system stability of the paralleled-inverter system controlled by the ATSMC scheme can be guaranteed even in the presence of system uncertainties. This finishes the proof of Theorem 2.

Note that, only system uncertainties including parameter variations, DC voltage fluctuations, and load disturbances are considered in the dynamic model (4). If the kth slave inverter disconnects from or reconnects to the parallel-inverter system, the implementation of the ATSMC algorithm just needs to remove or add the corresponding kth line of the vectors ($\boldsymbol{x}$, $\dot{x}^{ref}$, $\boldsymbol{z}$, $\boldsymbol{s}$, $\boldsymbol{e}$, $\boldsymbol{u}_b$, $\boldsymbol{u}_c$, $\boldsymbol{u}_{ca}$), the corresponding kth line and the kth column of the matrices ($\mathbf{A}_{pn}$, $\mathbf{B}_{pn}^{-1}$, $\mathbf{C}_{pn}$, $\mathbf{K}_s$), and the corresponding kth line and the $(k+1)$th column of $\mathbf{J}$ in (10) and (13). Then, the corresponding derivations remain valid such that the parallel-inverter system with the ATSMC scheme is still stable under the occurrence of structure uncertainties.

The designed ATSMC scheme achieves global robustness for the parallel-inverter system, and the chattering caused by the sign function in the TSMC can be relieved by the adaptive gain. However, detailed dynamic information of the parallel-inverter system is mandatory to ensure a favorable control property. Moreover, the control parameters of

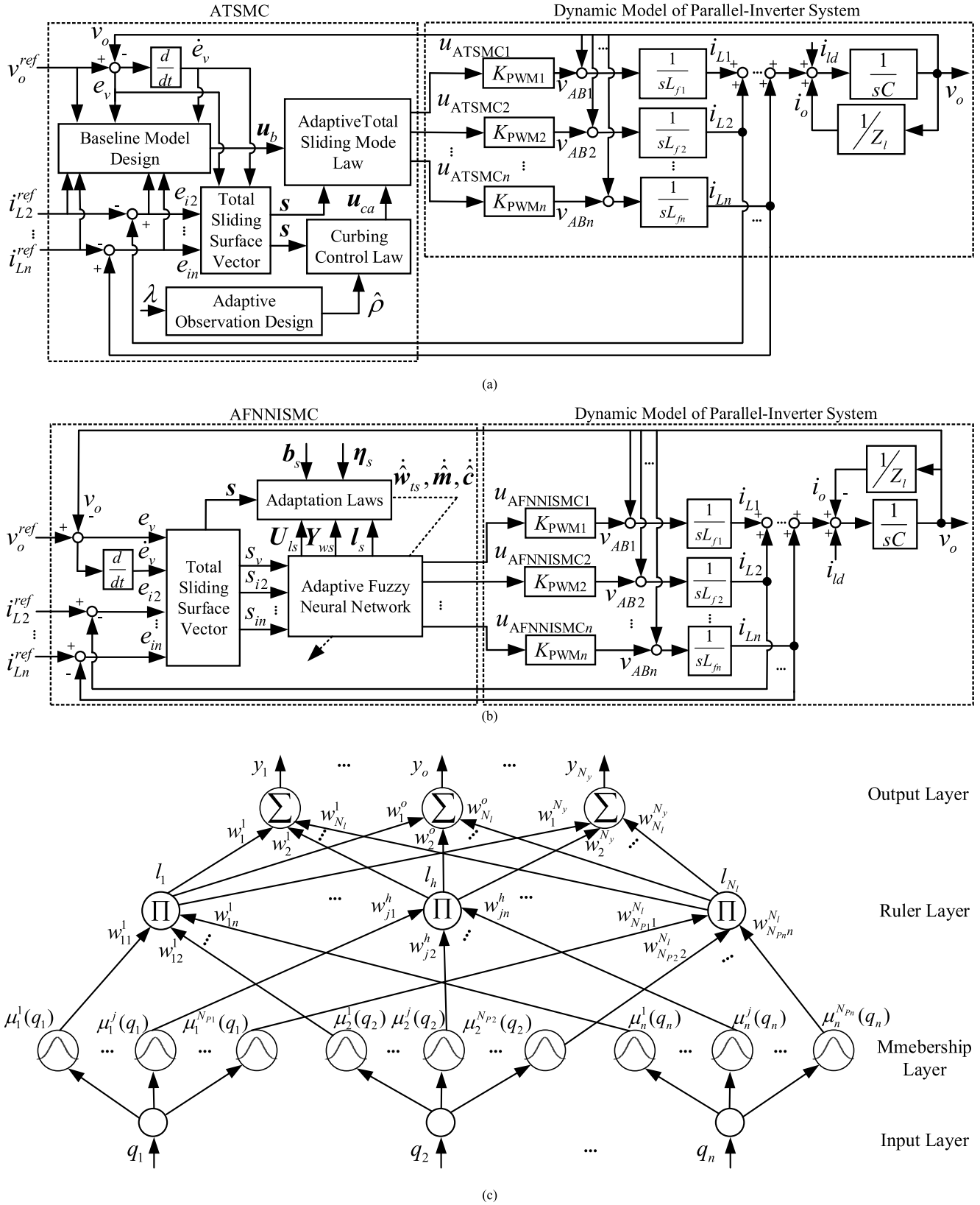

FIGURE 2. (a) Block diagram of designed ATSMC system; (b) Block diagram of proposed AFNNISMC scheme; (c) Structure of four-layer FNN.

the sliding-surface vector in (10) should be selected by a trial-and-error process. An adaptive fuzzy-neural-network-imitating sliding-mode control (AFNNISMC) strategy by using a fuzzy neural network (FNN) to imitate the TSMC law will be further developed for the parallel-inverter system in this study. The implementation of the proposed AFNNISMC strategy will be independent of detailed system information. Moreover, network parameters can be adjusted via adaptive laws, which can significantly eliminate the chattering phenomena in the TSMC and improve the robust characteristic of the parallel-inverter system no matter system uncertainties exist or not. The design of the proposed AFNNISMC framework will be described in the following section.

IV. AFNNISMC DESIGN

This section constructs an adaptive fuzzy-neural-network-imitating sliding-mode control (AFNNISMC) framework for a parallel-inverter system shown in Fig. 2(b). A four-layer fuzzy neural network (FNN) structure in Fig. 2(c) to be used for the proposed AFNNISMC scheme composes input, membership, rule, and output layers. In order to possess all information of error and its derivative, and reduce the network size, the elements in the sliding-surface vector are selected as the input signals of the FNN in this study to replace all tracking errors as input signal in conventional strategies. Moreover, the role of the second layer is to improve the classification ability via Gaussian activation functions. In addition, the rule layer is used to carry out fuzzy inference mechanisms, and the FNN outputs n control efforts ($u_{\text{AFNNISMC}1}$ and $u_{\text{AFNNISMC}k}|_{k=2,\cdots,n}$) for the parallel-inverter system. Furthermore, the parameters in the FNN can be adjusted online to improve the transient performance. The detailed description for the propagation of signals, functions used in the FNN, and the corresponding adaptation laws are studied as follows.

1) Input Layer: The input layer transmits input variables $q_i|_{i=1,\cdots,n}$ to the next layer. Unlike the conventional NN-based control, elements in the sliding-surface vector instead of errors and the derivatives of errors are selected as the input variable, which can significantly reduce the complexity and computational burden of the network.
2) Membership layer: Membership layer maps the input variables to fuzzy sets with the Gaussian membership functions as follows:

$$\mu_i^j(q_i) = \exp[-(q_i - m_i^j)^2 \Big/ (c_i^j)^2]\Big|_{j=1,\cdots,N_{pi}} \quad (16)$$

where N_{pi} denotes the number of membership functions for the ith input variable q_i; $\exp(\cdot)$ is an exponential function; m_i^j and c_i^j are the mean and standard deviation of the jth Gaussian function for the ith input, respectively. Parameter vectors ($\boldsymbol{m}$ and $\boldsymbol{c}$) are used to collect all the means and standard deviations as $\boldsymbol{m} = [\boldsymbol{m}_1 \cdots \boldsymbol{m}_i \cdots \boldsymbol{m}_n]^T \in \boldsymbol{R}^{N_r \times 1}$, in which $\boldsymbol{m}_i = [m_i^1 \cdots m_i^{N_{pi}}]^T\Big|_{i=1,\cdots,n} \in \boldsymbol{R}^{N_{pi}\times 1}$ and $N_r = \sum_{i=1}^{n} N_{p_i}$ denotes the total number of neurons in the membership layer;$\boldsymbol{c} = [\boldsymbol{c}_1 \cdots \boldsymbol{c}_i \cdots \boldsymbol{c}_n]^T \in \boldsymbol{R}^{N_r \times 1}$, in which $\boldsymbol{c}_i = [c_i^1 \cdots c_i^{N_{pi}}]^T\Big|_{i=1,\cdots,n} \in \boldsymbol{R}^{N_{pi}\times 1}$.
3) Rule layer: The output of the hth neuron in this layer is defined as the weighted multiplication of n input signals, which is labeled as l_h in (17). The input signals in this layer are the corresponding output of every Gaussian membership function in the previous layer.

$$l_h = \prod_{i=1}^{n} w_{ji}^h \mu_i^j(q_i)\Big|_{h=1,\cdots,N_l} \quad (17)$$

where N_l is the total number of output neurons; all values of l_h are gathered by a vector $\boldsymbol{l} = \begin{bmatrix} l_1 l_2 \cdots l_{N_l} \end{bmatrix} \in R^{N_l \times 1}$; w_{ji}^h is the weight between the ruler layer and the previous membership layer, which is assumed to be unity in this study.
4) Output layer: The output node $y_o|_{o=1,\cdots,N_y}$ sums all input signals of this layer as the output, which can be expressed as

$$y_o = \sum_{h=1}^{N_l} w_h^o l_h \quad (18)$$

where w_h^o is the weight between the oth output signal in the output layer and the hth output signal in the rule layer. In this layer, the weights can be collected by the following weight matrix ($\mathbf{W}$):

$$\mathbf{W} = \begin{bmatrix} w_1^1 & w_2^1 & \cdots & w_{N_l}^1 \\ w_1^2 & w_2^2 & \cdots & w_{N_l}^2 \\ \vdots & \vdots & \ddots & \vdots \\ w_1^{N_y} & w_2^{N_y} & \cdots & w_{N_l}^{N_y} \end{bmatrix} = [\boldsymbol{w}_1 \cdots \boldsymbol{w}_o \cdots \boldsymbol{w}_{Ny}]^T \quad (19)$$

where $\boldsymbol{w}_o = [w_1^o w_2^o \cdots w_{N_l}^o] \in R^{1\times N_l}$. Moreover, the outputs of the FNN can be re-expressed by the following output vector ($\boldsymbol{y}$):

$$\boldsymbol{y} = [y_1 \;\; y_2 \;\; \cdots \;\; y_{N_y}]^T = \boldsymbol{u}_{\text{AFNNISMC}}(\boldsymbol{q}, \mathbf{W}, \boldsymbol{m}, \boldsymbol{c}) \quad (20)$$

Assumption 2: There are optimal weight matrix ($\mathbf{W}^*$), mean vectors ($\boldsymbol{m}^*$), and standard deviation vectors ($\boldsymbol{c}^*$) for an FNN ($\boldsymbol{u}_{\text{AFNNISMC}}^*$) to approximate the TSMC law ($\boldsymbol{u}_{\text{TSMC}}$) in (10) due to the powerful approximation ability of the FNN. Then, the TSMC law ($\boldsymbol{u}_{\text{TSMC}}$) can be rewritten as

$$\boldsymbol{u}_{\text{TSMC}} = \boldsymbol{u}_{\text{AFNNISMC}}^*(\boldsymbol{q}, \mathbf{W}^*, \boldsymbol{m}^*, \boldsymbol{c}^*) + \boldsymbol{\varepsilon}_s \quad (21)$$

where $\boldsymbol{\varepsilon}_s$ is defined as the minimum reconstructed-error vector between $\boldsymbol{u}_{\text{AFNNISMC}}^*$ and $\boldsymbol{u}_{\text{TSMC}}$.

The actual control law of the proposed AFNNISMC to imitate the TSMC law ($\boldsymbol{u}_{\text{TSMC}}$) is designed as

$$\hat{\boldsymbol{u}}_{\text{AFNNISMC}}(\boldsymbol{q},\ \hat{\mathbf{W}},\ \hat{\boldsymbol{m}},\ \hat{\boldsymbol{c}}) = \hat{W}\hat{\boldsymbol{l}} \quad (22)$$

where $\hat{\mathbf{W}}$, $\hat{\boldsymbol{m}}$, and $\hat{\boldsymbol{c}}$ are the estimated values of $\mathbf{W}^*$, $\boldsymbol{m}^*$, and $\boldsymbol{c}^*$, respectively, with the adaptive online learning ability to

be designed later; $\hat{\boldsymbol{l}}$ is the estimated vector of $\boldsymbol{l}^*$. By subtracting (22) from (21), the approximation error ($\tilde{\boldsymbol{u}}_s$) can be expressed as

$$\begin{aligned}\tilde{\boldsymbol{u}}_s &= \boldsymbol{u}_{\text{TSMC}} - \hat{\boldsymbol{u}}_{\text{AFNNISMC}} \\ &= \boldsymbol{u}^*_{\text{AFNNISMC}} + \boldsymbol{\varepsilon}_s - \hat{\boldsymbol{u}}_{\text{AFNNISMC}}\end{aligned} \tag{23}$$

For ease of stability analyses, the activation and membership functions of the FNN are transformed into partially linear forms by the Taylor series expansion in this study. The corresponding approximation error in (23) can be represented as

$$\begin{aligned}\tilde{\boldsymbol{u}}_s &= \begin{bmatrix} \frac{\partial \hat{u}_{\text{AFNNISMC1}}}{\partial \hat{\boldsymbol{w}}_1}|_{\hat{\boldsymbol{w}}_1=\boldsymbol{w}_1^*}(\boldsymbol{w}_1^{*T} - \hat{\boldsymbol{w}}_1^T) + h_{ws1} \\ \vdots \\ \frac{\partial \hat{u}_{\text{AFNNISMC}y}}{\partial \hat{\boldsymbol{w}}_{N_y}}|_{\hat{\boldsymbol{w}}_{N_y}=\boldsymbol{w}_{N_y}^*}(\boldsymbol{w}_{N_y}^{*T} - \hat{\boldsymbol{w}}_{N_y}^T) + h_{wsN_y} \end{bmatrix} \\ &\quad + \begin{bmatrix} \frac{\partial \hat{u}_{\text{AFNNISMC1}}}{\partial \hat{\boldsymbol{l}}^T} \\ \vdots \\ \frac{\partial \hat{u}_{F\,\text{AFNNISMC}N_y}}{\partial \hat{\boldsymbol{l}}^T} \end{bmatrix}|_{\hat{\boldsymbol{l}}=\boldsymbol{l}^*}(\boldsymbol{l}^* - \hat{\boldsymbol{l}}) + \begin{bmatrix} h_{ls1} \\ \vdots \\ h_{lsN_y} \end{bmatrix} + \boldsymbol{\varepsilon}_s \\ &= \begin{bmatrix} \boldsymbol{y}_{ws1}\tilde{\boldsymbol{w}}_1^T \\ \vdots \\ \boldsymbol{y}_{wsN_y}\tilde{\boldsymbol{w}}_{N_y}^T \end{bmatrix} + \boldsymbol{h}_{ws} + \begin{bmatrix} \boldsymbol{u}_{ls1} \\ \vdots \\ \boldsymbol{u}_{lsN_y} \end{bmatrix}\tilde{\boldsymbol{l}} + \boldsymbol{h}_{ls} + \boldsymbol{\varepsilon}_s \\ &= \mathbf{Y}_{ws}\tilde{\boldsymbol{w}}_{ts} + \mathbf{U}_{ls}\tilde{\boldsymbol{l}} + \boldsymbol{v}_s\end{aligned} \tag{24}$$

where $\tilde{\boldsymbol{w}}_{ts} = \boldsymbol{w}_{ts}^* - \hat{\boldsymbol{w}}_{ts} = [\tilde{\boldsymbol{w}}_1^T, \cdots, \tilde{\boldsymbol{w}}_o^T, \cdots, \tilde{\boldsymbol{w}}_{Ny}^T]^T \in R^{N_{ly}\times 1}$, in which $\tilde{\boldsymbol{w}}_o = \boldsymbol{w}_o^* - \hat{\boldsymbol{w}}_o \in R^{1\times N_l}$ and $N_{ly} = N_l \times N_y$; $\tilde{\boldsymbol{l}} = \boldsymbol{l}^* - \hat{\boldsymbol{l}} \in R^{N_l\times 1}$; $\boldsymbol{w}_{ts}^*$ and $\boldsymbol{l}^*$ are the optimum vectors of $\boldsymbol{w}_{ts}$ and $\boldsymbol{l}$, $\hat{\boldsymbol{w}}_{ts}$ and $\hat{\boldsymbol{l}}$ are the estimated vectors of $\boldsymbol{w}_{ts}^*$ and $\boldsymbol{l}^*$; $\boldsymbol{h}_{ws} \in R^{N_y\times 1}$ and $\boldsymbol{h}_{ls} \in R^{N_y\times 1}$ are higher order terms in Taylor series; $\mathbf{Y}_{ws} = \text{diag}(\boldsymbol{y}_{ws1}, \boldsymbol{y}_{ws2}, \cdots, \boldsymbol{y}_{wsN_y}) \in R^{N_y\times N_{ly}}$; $\boldsymbol{U}_{ls} = [u_{ls1}, u_{ls2}, \cdots, u_{lsN_y}]^T \in R^{N_y\times N_l}$; $\boldsymbol{v}_s = \boldsymbol{h}_{ws} + \boldsymbol{h}_{ls} + \boldsymbol{\varepsilon}_s$.

Moreover, the linear form of $\tilde{\boldsymbol{l}}$ can be expressed as

$$\begin{aligned}\tilde{\boldsymbol{l}} &= \begin{bmatrix}\tilde{l}_1 & \tilde{l}_2 \cdots \tilde{l}_{N_l}\end{bmatrix}^T = \begin{bmatrix} \frac{\partial \hat{l}_1}{\partial \hat{\boldsymbol{m}}^T} \\ \frac{\partial \hat{l}_2}{\partial \hat{\boldsymbol{m}}^T} \\ \vdots \\ \frac{\partial \hat{l}_{N_l}}{\partial \hat{\boldsymbol{m}}^T} \end{bmatrix}|_{\hat{\boldsymbol{m}}=\boldsymbol{m}^*}(\boldsymbol{m}^* - \hat{\boldsymbol{m}}) \\ &\quad + \begin{bmatrix} \frac{\partial \hat{l}_1}{\partial \hat{\boldsymbol{c}}^T} \\ \frac{\partial \hat{l}_2}{\partial \hat{\boldsymbol{c}}^T} \\ \vdots \\ \frac{\partial \hat{l}_{N_l}}{\partial \hat{\boldsymbol{c}}^T} \end{bmatrix}|_{\hat{\boldsymbol{c}}=\boldsymbol{c}^*}(\boldsymbol{c}^* - \hat{\boldsymbol{c}}) + \boldsymbol{h}_{mcs} \\ &\equiv \boldsymbol{l}_{ms}\tilde{\boldsymbol{m}} + \boldsymbol{l}_{cs}\tilde{\boldsymbol{c}} + \boldsymbol{h}_{mcs}\end{aligned} \tag{25}$$

where

$$\boldsymbol{l}_{ms} = \begin{bmatrix} \frac{\partial \hat{l}_1}{\partial \hat{\boldsymbol{m}}} \frac{\partial \hat{l}_2}{\partial \hat{\boldsymbol{m}}} \cdots \frac{\partial \hat{l}_{N_l}}{\partial \hat{\boldsymbol{m}}} \end{bmatrix}^T |_{\hat{\boldsymbol{m}}=\boldsymbol{m}^*} \in R^{N_l\times N_r}, \tilde{\boldsymbol{m}} = \boldsymbol{m}^* - \hat{\boldsymbol{m}},$$

$$\boldsymbol{l}_{cs} = \begin{bmatrix} \frac{\partial \hat{l}_1}{\partial \hat{\boldsymbol{c}}} \frac{\partial \hat{l}_2}{\partial \hat{\boldsymbol{c}}} \cdots \frac{\partial \hat{l}_{N_l}}{\partial \hat{\boldsymbol{c}}} \end{bmatrix}^T |_{\hat{\boldsymbol{c}}=\boldsymbol{c}^*} \in R^{N_l\times N_r}, \quad \tilde{\boldsymbol{c}} = \boldsymbol{c}^* - \hat{\boldsymbol{c}},$$

$\boldsymbol{h}_{mcs} \in R^{N_l\times 1}$ is a vector of higher-order terms. By substituting (25) into (24), the approximation error ($\tilde{\boldsymbol{u}}_s$) can be rewritten as

$$\tilde{\boldsymbol{u}}_s = \mathbf{Y}_{ws}\tilde{\boldsymbol{w}}_{ts} + \mathbf{U}_{ls}\boldsymbol{l}_{ms}\tilde{\boldsymbol{m}} + \mathbf{U}_{ls}\boldsymbol{l}_{cs}\tilde{\boldsymbol{c}} + \boldsymbol{y}_s' \tag{26}$$

where $\boldsymbol{y}_s' = \boldsymbol{v}_s + \mathbf{U}_{ls}\boldsymbol{h}_{mcs}$.

Theorem 3: For the parallel-inverter system in (4), if the proposed AFNNISMC law is designed as (22) with the corresponding adaptation laws for FNN parameters in (27)-(29), the total sliding-surface vector will converge to zero asymptotically. Moreover, the convergence of the network parameters and the system stability of the proposed AFNNISMC scheme can be assured.

$$\begin{cases} \text{If } (\|\hat{\boldsymbol{w}}_{ts}\| < b_{ws}) \text{ or } (\|\hat{\boldsymbol{w}}_{ts}\| = b_{ws} \text{ and } \boldsymbol{s}^T\mathbf{Y}_{ws}\hat{\boldsymbol{w}}_{ts} \le 0) \\ \quad \dot{\hat{\boldsymbol{w}}}_{ts} = \eta_{ws}(\boldsymbol{s}^T\mathbf{Y}_{ws})^T \end{cases} \tag{27a}$$

$$\begin{cases} \text{If } (\|\hat{\boldsymbol{w}}_{ts}\| = b_{ws} \text{ and } \boldsymbol{s}^T\mathbf{Y}_{ws}\hat{\boldsymbol{w}}_{ts} > 0) \\ \quad \dot{\hat{\boldsymbol{w}}}_{ts} = \eta_{ws}[\boldsymbol{s}^T\mathbf{Y}_{ws} - (\boldsymbol{s}^T\mathbf{Y}_{ws}\hat{\boldsymbol{w}}_{ts}\hat{\boldsymbol{w}}_{ts}^T / \|\hat{\boldsymbol{w}}_{ts}\|^2)]^T \end{cases} \tag{27b}$$

$$\begin{cases} \text{If } (\|\hat{\boldsymbol{m}}\| < b_{ms}) \text{ or } (\|\hat{\boldsymbol{m}}\| = b_{ms} \text{ and } \boldsymbol{s}^T\mathbf{U}_{ls}\boldsymbol{l}_{ms}\hat{\boldsymbol{m}} \le 0) \\ \quad \dot{\hat{\boldsymbol{m}}} = \eta_{ms}(\boldsymbol{s}^T\mathbf{U}_{ls}\boldsymbol{l}_{ms})^T \end{cases} \tag{28a}$$

$$\begin{cases} \text{If } (\|\hat{\boldsymbol{m}}\| = b_{ms} \text{ and } \boldsymbol{s}^T\mathbf{U}_{ls}\boldsymbol{l}_{ms}\hat{\boldsymbol{m}} > 0) \\ \quad \dot{\hat{\boldsymbol{m}}} = \eta_{ms}[\boldsymbol{s}^T\mathbf{U}_{ls}\boldsymbol{l}_{ms} - (\boldsymbol{s}^T\mathbf{U}_{ls}\boldsymbol{l}_{ms}\hat{m}\hat{m}^T / \|\hat{\boldsymbol{m}}\|^2)]^T \end{cases} \tag{28b}$$

$$\begin{cases} \text{If } (\|\hat{\boldsymbol{c}}\| < b_{cs}) \text{ or } (\|\hat{\boldsymbol{c}}\| = b_{cs} \text{ and } \boldsymbol{s}^T\mathbf{U}_{ls}\boldsymbol{l}_{cs}\hat{\boldsymbol{c}} \le 0) \\ \quad \dot{\hat{\boldsymbol{c}}} = \eta_{cs}(\boldsymbol{s}^T\mathbf{U}_{ls}\boldsymbol{l}_{cs})^T \end{cases} \tag{29a}$$

$$\begin{cases} \text{If } (\|\hat{\boldsymbol{c}}\| = b_{cs} \text{ and } \boldsymbol{s}^T\mathbf{U}_{ls}\boldsymbol{l}_{cs}\hat{\boldsymbol{c}} > 0) \\ \quad \dot{\hat{\boldsymbol{c}}} = \eta_{cs}\left[\boldsymbol{s}^T\mathbf{U}_{ls}\boldsymbol{l}_{cs} - (\boldsymbol{s}^T\mathbf{U}_{ls}\boldsymbol{l}_{cs}\hat{c}\hat{c}^T / \|\hat{\boldsymbol{c}}\|^2)^T\right] \end{cases} \tag{29b}$$

where η_{ws}, η_{ms}, and η_{cs} are positive learning rates; b_{ws}, b_{ms}, and b_{cs} are given positive bound values; $\|\cdot\|$ denotes the Euclidean norm operator. In Fig. 2(b), $\boldsymbol{\eta}_s = [\eta_{ws}\eta_{ms}\eta_{cs}]$ is a give positive learning-rate vector; $b_s = [b_{ws}b_{ms}b_{cs}]$ is a given positive bound vector.

Proof: Define a third Lyapunov function as

$$V_{\text{AFNNISMC}}(\boldsymbol{s}, \tilde{\boldsymbol{w}}_{ts}, \tilde{\boldsymbol{m}}, \tilde{\boldsymbol{c}}) = \frac{1}{2}\boldsymbol{s}^T\boldsymbol{s} + \frac{\tilde{\boldsymbol{w}}_{ts}^T\tilde{\boldsymbol{w}}_{ts}}{2\eta_{ws}} + \frac{\tilde{\boldsymbol{m}}^T\tilde{\boldsymbol{m}}}{2\eta_{ms}} + \frac{\tilde{\boldsymbol{c}}^T\tilde{\boldsymbol{c}}}{2\eta_{cs}} \tag{30}$$

By substituting (9) into the derivative of (30), substituting the actual control law of the AFNNISMC ($\hat{\boldsymbol{u}}_{\text{AFNNISMC}}$) in (22) into the control effort ($\boldsymbol{u}$) in (4), and using adaptation laws for network parameters in (27)-(29), one can obtain

$$\begin{aligned}&\dot{V}_{\text{AFNNISMC}} \\ &= \boldsymbol{s}^T\mathbf{B}_{pn}^{-1}[-\rho\,\text{sgn}(\boldsymbol{s}) - \mathbf{K}_s\boldsymbol{s} - \boldsymbol{\psi} + \mathbf{B}_{pn}\boldsymbol{y}_s'] \\ &\quad + V_{ws} + V_{ms} + V_{cs} \\ &\le -\boldsymbol{s}^T\mathbf{B}_{pn}^{-1}\mathbf{K}_s\boldsymbol{s} - \left\|\boldsymbol{s}^T\mathbf{B}_{pn}^{-1}\right\|_1[\rho - \|\mathbf{B}_{pn}\boldsymbol{y}_s' - \boldsymbol{\psi}\|_1] \\ &\le -\boldsymbol{s}^T\mathbf{B}_{pn}^{-1}\mathbf{K}_s\boldsymbol{s} \le 0\end{aligned} \tag{31}$$

where $V_{ws} = \boldsymbol{s}^T\mathbf{Y}_{ws}\tilde{\boldsymbol{w}}_{ts} - \frac{\dot{\tilde{\boldsymbol{w}}}_{ts}^T\tilde{\boldsymbol{w}}_{ts}}{\eta_{ws}}$, $V_{ms} = \boldsymbol{s}^T\mathbf{U}_{ls}\boldsymbol{l}_{ms}\tilde{\boldsymbol{m}} - \frac{\dot{\tilde{\boldsymbol{m}}}^T\tilde{\boldsymbol{m}}}{\eta_{ms}}$, and $V_{cs} = \boldsymbol{s}^T\mathbf{U}_{ls}\boldsymbol{l}_{cs}\tilde{\boldsymbol{c}} - \frac{\dot{\tilde{\boldsymbol{c}}}^T\tilde{\boldsymbol{c}}}{\eta_{cs}}$. The detailed derivation process of (31) can be referred to the Appendix. From (31), the derivative of the third Lyapunov function $\dot{V}_{\text{AFNNISMC}}(\boldsymbol{s}, \tilde{\boldsymbol{w}}_{ts}, \tilde{\boldsymbol{m}}, \tilde{\boldsymbol{c}})$ is a negative semi-definite function because of $\dot{V}_{\text{AFNNISMC}}(\boldsymbol{s}, \tilde{\boldsymbol{w}}_{ts}, \tilde{\boldsymbol{m}}, \tilde{\boldsymbol{c}}) \leq 0$, i.e., $V_{\text{AFNNISMC}}(\boldsymbol{s}(t), \tilde{\boldsymbol{w}}_{ts}, \tilde{\boldsymbol{m}}, \tilde{\boldsymbol{c}}) \leq V_{\text{AFNNISMC}}(\boldsymbol{s}(0), \tilde{\boldsymbol{w}}_{ts}, \tilde{\boldsymbol{m}}, \tilde{\boldsymbol{c}})$. It indicates that $\boldsymbol{s}, \tilde{\boldsymbol{w}}_{ts}, \tilde{\boldsymbol{m}}$ and $\tilde{\boldsymbol{c}}$ are bounded functions. According to the Lyapunov stability theory and the Barbalat's lemma [33], it can conclude that $\boldsymbol{s}(t), \tilde{\boldsymbol{w}}_{ts}, \tilde{\boldsymbol{m}}$ and $\tilde{\boldsymbol{c}}$ will converge to zero as time tends to infinity. Thus, the stability of the proposed AFNNISMC system for the parallel-inverter system can be guaranteed without auxiliary compensators in conventional intelligent control. This finishes the proof of Theorem 3.

Note that, when the disconnected signal of the slave inverter is detected, the input signal from the disconnection-inverter for the FNN is set to zero, and the output of the corresponding neuron in the membership layer of the FNN remains unchanged. Disconnection or re-connection of someone slave inverter does not change the structure of the network in the proposed AFNNISMC. Therefore, the AFNNISMC system can work well even under the occurrence of the structure change in the paralleled-inverter system.

V. NUMERICAL SIMULATIONS AND EXPERIMENTAL VERIFICATION

In this study, numerical simulations and experimental examinations of a parallel-inverter system with two single-inverter units are carried out to demonstrate the superiority of the proposed adaptive fuzzy-neural-network-imitating sliding-mode control (AFNNISMC) system. The nominal values of circuit parameters in this parallel-inverter system are summarized in Table 2.

The main objective of the proposed AFNNISMC system for the parallel-inverter system is to obtain the robust property of high-precision voltage tracking and current sharing under system uncertainties. The input signals of the fuzzy neural network (FNN) are the elements of the sliding-surface vector (s_v and s_{i2}), i.e., $q_1 = s_v$ and $q_2 = s_{i2}$ ($n = 2$). Moreover, the FNN outputs are control efforts ($u_{\text{AFNNISMC1}}$ and $u_{\text{AFNNISMC2}}$) for the master inverter and the slave inverter, respectively ($N_y = 2$). The fuzzy sets for each input signal in this study are equally divided into three parts by the Gaussian function ($N_{p1} = N_{p2} = 3$). The total number of nodes in the rule layer is nine ($N_l = 9$). Thus, there are 2, 6, 9, and 2 neurons in the four-layer FNN structure. In general, initial values of network parameters in the FNN are roughly set based on expert knowledge.

In order to facilitate the selection of controller parameters for obtaining better control performance, state variables are normalized to eliminate the influence of two inputs in different levels (i.e., the voltage sliding surface and the current sliding surface, s_v and s_{i2}). Because initial values of network parameters can be adjusted by online adaptation laws, initial

TABLE 2. Nominal Values of Circuit Parameters in Parallel-Inverter System.

Circuit parameters of inverters	Master	Slave
DC source voltage	200V	200V
AC Bus voltage (RMS)	110V	
Inductance of LC filter	2mH	2mH
Equivalent resistance of Inductance	0.2Ω	0.2Ω
Capacitance of LC filter	20μF	20μF
Fundamental Frequency	60Hz	
Switching Frequency	20kHz	
Resistance Load	12.5Ω	
RC Load	12.5Ω / 96μF	
RCD Nonlinear Load	12.5Ω /1100μF /KBPC3506P	

weight vectors ($\boldsymbol{w}_1$ and $\boldsymbol{w}_2$) in the FNN are set to zero; initial mean vectors ($\boldsymbol{m}_1$ and $\boldsymbol{m}_2$) are all set as [-30 0 30], and initial standard deviation vectors ($\boldsymbol{c}_1$ and $\boldsymbol{c}_2$) are all selected as [30 30 30]. Moreover, control parameters in the proposed AFNNISMC are selected as follows:

$$\begin{aligned} \mathbf{J}_v &= [0.80.3;\ 10]\,, \quad \mathbf{J}_i = [1.1080;\ 0\ 0.2] \\ \eta_{w1s} &= 0.258,\ \eta_{m1s} = \eta_{c1s} = 1.15 \times 10^{-6} \\ \eta_{w2s} &= 2.503,\ \eta_{m2s} = \eta_{c2s} = 1.55 \times 10^{-6} \end{aligned} \tag{32}$$

An adaptive total sliding-mode control (ATSMC) scheme in Section III is also performed for a comparison with the proposed AFNNISMC strategy. In fairness, control parameters of the designed ATSMC are determined to obtain a similar control performance with that of the proposed AFNNISMC at the nominal case. The conservative selection of $\mathbf{J}_v = [8 \times 10^7\ 5 \times 10^3;\ 1\ 0]$ and $\mathbf{J}_i = [4.2 \times 10^3\ 0;\ 0\ 4.2 \times 10^3]$ in the designed ATSMC are set to cope with the coefficients of state equations ($\mathbf{A}_{pn}$, $\mathbf{B}_{pn}$, and $\mathbf{C}_{pn}$), which are different from the vectors in the model-free AFNNISMC scheme. Moreover, the value of $\mathbf{K}_s = [1500\ 0;\ 0\ 1015]$ in (13a) is chosen to ensure the stability of the designed ATSMC system, even for the worst case of $\rho < \|\boldsymbol{\psi}\|_1$. In addition, the value of $\lambda = 200$ is selected for the adaptation in (13b).

By taking a parallel-inverter system with a master inverter and a slave inverter as example, four kinds of disturbances are considered in this study. According to the parameters in Table 2, the upper bound (ρ) of the lumped uncertainty vector can be roughly calculated according to (5). By considering the load variations from $R_l = 12.5\Omega$ to $R_l = 25\Omega$, the structure uncertainty of the slave inverter to be reconnected into the master inverter, the input voltage fluctuation of the slave inverter ($V_{dc1} = 200$V; V_{dc2} changes from 200V to 180V), and the values of filter inductors (L_{f1} and L_{f2}) deviated by –10%, theoretical upper bounds (ρ) of the lumped uncertainty vector can be roughly obtained for the above four variations to be about 24.6, 26.2, 3.44 and 2.29, respectively. Although the upper bound (ρ) of the lumped uncertainty vector can be conservatively selected as 26.2, it will result in a serious chattering control effort. Thanks to the introduction of $\mathbf{B}_{pn}^{-1}\mathbf{K}_s\boldsymbol{s}$ into the curbing control law (10c), the conservative

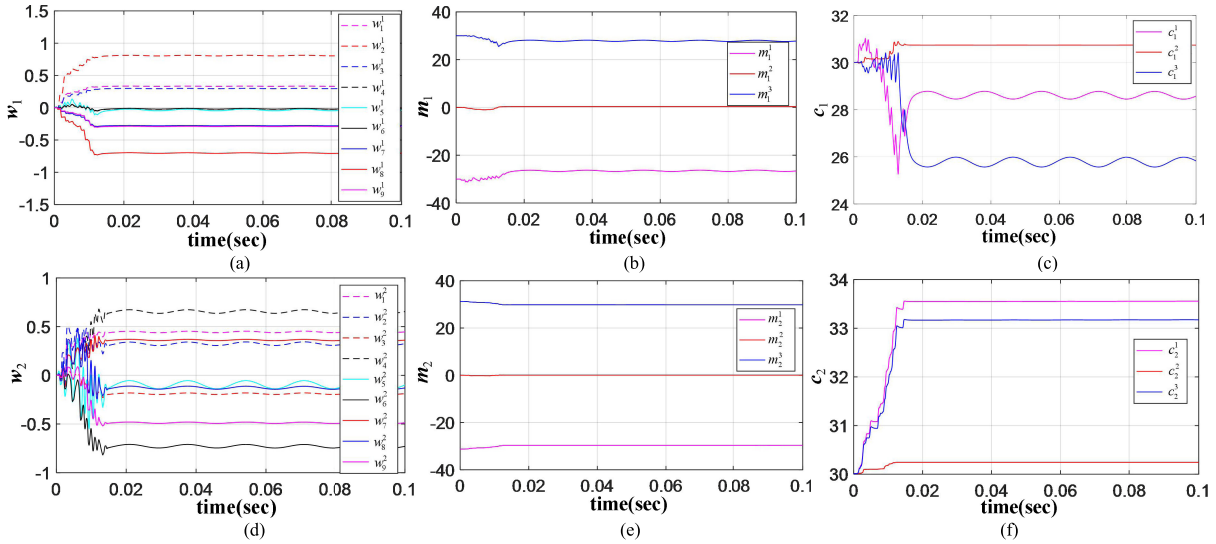

FIGURE 3. Adaptive adjustment curves of parameters in AFNNISMC: (a) Weigh vector adaption (w_1); (b) Weigh vector adaption (w_2); (c) Mean vector adaption (m_1); (d) Mean vector adaption (m_2); (e) Standard deviation vector adaption (c_1); (f) Standard deviation vector adaption (c_2).

selection of the gain matrix ($\mathbf{K}_s$) to cover with an insufficient upper bound (i.e., a smaller value ρ) is helpful to reduce the chattering phenomena introduced by the sign function.

The control performance of the designed ATSMC and the proposed AFNNISMC are examined by the following normalized-mean-square-error (NMSE) values of the voltage tracking and current sharing:

$$\text{NMSE}(x) = \frac{1}{x_{\max} T} \sum_{n=1}^{T} x^2(n) \tag{33}$$

where x is the voltage tracking error (e_v) or the current sharing error (e_i); $x_{\max}$ is the maximum value of the sinusoidal voltage or current command; T is the sampling interval.

A. NUMERICAL SIMULATIONS

The numerical simulation model of a parallel-inverter system in an island micro-grid (MG) is built by the Matlab software. The current command of the slave inverter is equal to the current of the master inverter. The superiority in voltage tracking and current sharing by the proposed AFNNISMC will be validated by comparing with the performance of the designed ATSMC. Four simulated conditions are considered: 1) Two inverters are operated in parallel at the beginning ($R_l = 25\Omega$, $V_{dc1} = V_{dc2} = 200$V, $L_{f1} = L_{f2} = 2$mH), and the load is varied at 0.172s (R_l changes from 25Ω to12.5Ω or from 12.5Ω to 25Ω); 2) The slave inverter disconnects from the master inverter at 0.1125s and re-connects at 0.304s; 3) The input voltage of the slave inverter fluctuates at $t = 0.171$ ($V_{dc1} = 200$V; V_{dc2} changes from 200V to 180V); 4) The value of the filter inductance is deviated ± 10% of the nominal value (2mH) in the slave inverter.

Figure 3 displays adaptive adjustment curves of network parameters in the proposed AFNNISMC. The weight vectors ($\boldsymbol{w}_1$ and $\boldsymbol{w}_2$), the mean vectors ($\boldsymbol{m}_1$ and $\boldsymbol{m}_2$), and the standard deviation vectors ($\boldsymbol{c}_1$ and $\boldsymbol{c}_2$) update online to steady-state values for obtaining satisfactory system responses, even though their values are roughly initialized. As can be seen from Fig. 3, it demonstrates that the proposed AFNNISMC scheme has good self-regulation ability.

The state trajectories in the parameter training process of the output voltage in the parallel-inverter system by the proposed AFNNISMC under the occurrence of system uncertainties are depicted in Fig. 4, where each trajectory is a circle centered at (0,0,0). The states deviate from the circle trajectory when the system uncertainties occur, and the corresponding state trajectories can return to the circle eventually. Moreover, the circle is dramatically decreased via the online training process. The black arrows point to the convergence direction of the output voltage state.

Figure 5 exhibits the simulated results of the voltage tracking and current sharing error of the parallel-inverter system by the proposed AFNNISMC and the designed ATSMC. As can be seen from Fig. 5, the errors by the designed ATSMC are similar to the ones by the proposed AFNNISMC during the steady state as shown in Fig. 5(a) and 5(d). Because of the shorter settling times and lower overshoots at startup by the proposed AFNNISMC, there are 59.7% and 92.8% improvement by the proposed AFNNISMC in the NMSE values of voltage tracking errors (0.0119 by the ATSMC and 0.0048 by the AFNNISMC) and current sharing errors (6.66×10^{-4} by the ATSMC and 4.80×10^{-5} by the AFNNISMC), respectively.

The transient tracking responses by the designed ATSMC scheme are more susceptible to load disturbances with larger overshoot and more chattering in the output voltage and filter inductor currents. As can be seen from Fig. 5(b) and 5(c), the NMSE values (0.0352 and 0.0366) of the voltage tracking error by the designed ATSMC can be reduced to

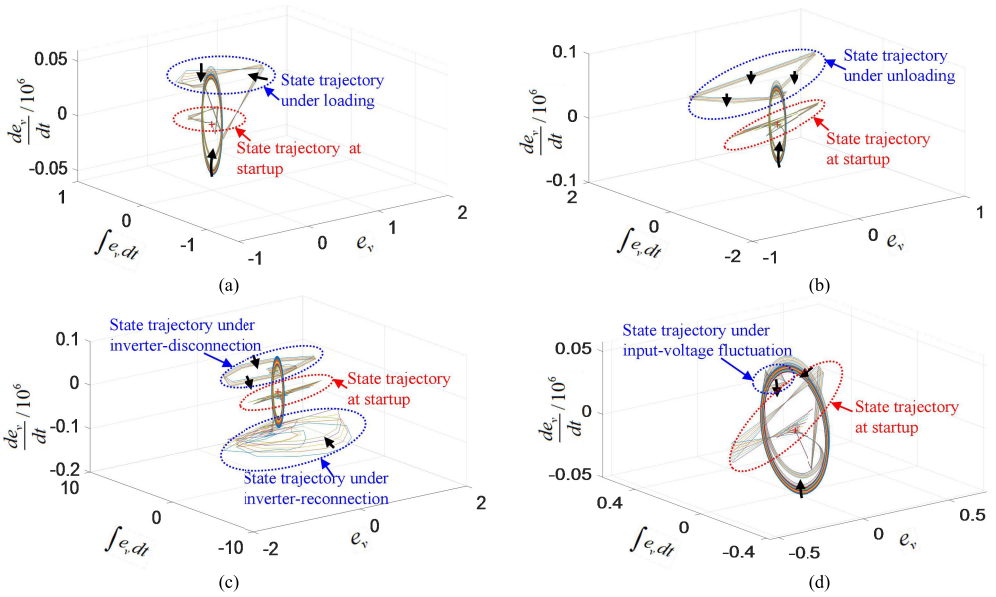

FIGURE 4. Output voltage state trajectory in parameter training of parallel-inverter system by AFNNISMC under system uncertainties: (a) Load variations from 25Ω to12.5Ω; (b) Load variation from 12.5Ω to25Ω; (c) Slave inverter disconnection and re-connection; (d) Input voltage variation of slave inverter (DC bus voltage changes from 200V to 180V).

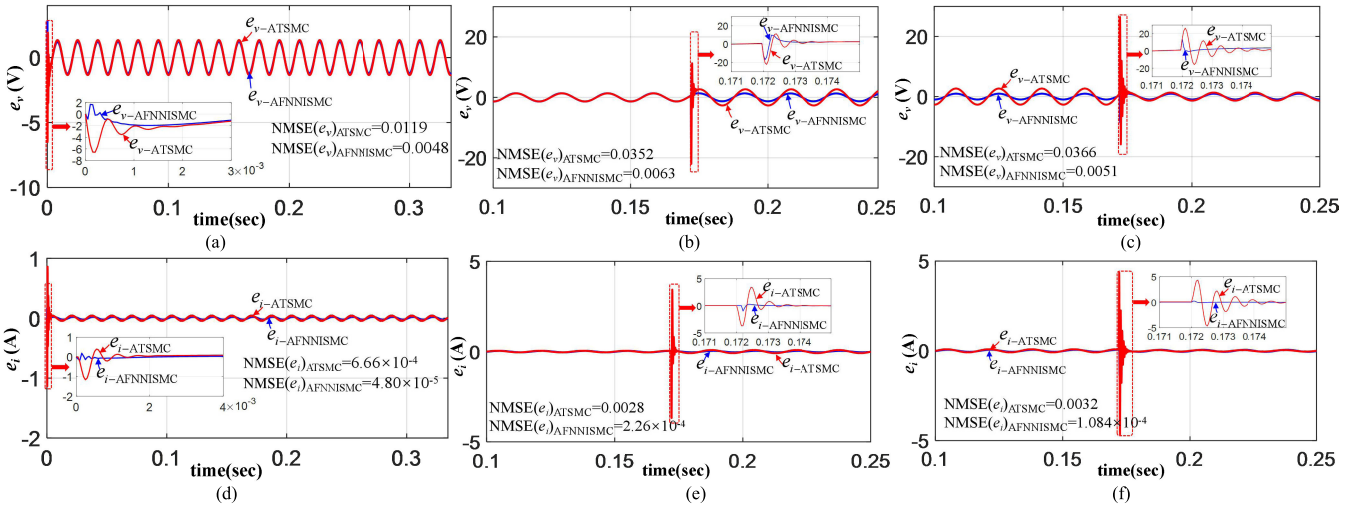

FIGURE 5. Simulated results of voltage tracking error and current sharing error of parallel-inverter system by AFNNISMC and ATSMC: (a) Tracking error of output voltage under $R_l = 25\Omega$; (b) Tracking error of output voltage under load changes from 25Ω to 12.5Ω; (c) Tracking error of output voltage under load changes from 12.5Ω to 25Ω; (d) Current sharing error under $R_l = 25\Omega$; (e) Current sharing error under load variation from 25Ω to 12.5Ω; (f) Current sharing error under load variation from 12.5Ω to 25Ω.

(0.0063 and 0.0051) by the proposed AFNNISMC under the occurrence of loading and unloading disturbance at $t = 0.172$s. By observing Fig. 5(e) and 5(f), the NMSE values (0.0028 and 0.0032) of the current sharing error by the designed ATSMC can be reduced to (2.26×10^{-4} and 1.084×10^{-4}) by the proposed AFNNISMC system. While the errors by the designed ATSMC are greater than the ones by the proposed AFNNISMC under a heavy load ($R_l = 12.5\Omega$) as shown in Fig. 5(b) and 5(c), it verifies that the control performance of the proposed model-free AFNNISMC is insensitive to load variations.

The simulated results of the parallel-inverter system by the designed ATSMC and the proposed AFNNISMC under the occurrence of disconnection and re-connection of the slave inverter are depicted in Fig. 6. The master inverter still can supply power solely after the slave inverter disconnects, and the parallel-inverter system remains workable, even the disconnection and re-connection operates at the worst case, e.g., the peak value or the valley of the output voltage. The corresponding NMSE value under disconnection and the cumulative NMSE value after the re-connection of the slave inverter are (0.015 and 0.049) by the designed ATSMC, and

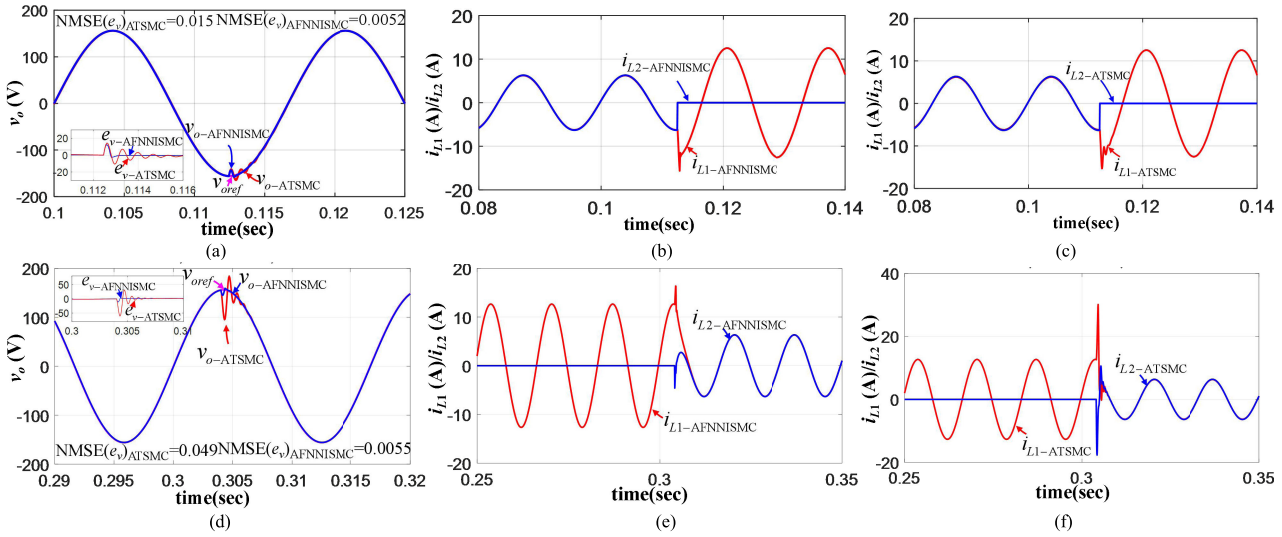

FIGURE 6. Simulated results of parallel-inverter system by AFNNISMC and ATSMC under disconnection and re-connection of slave inverter: (a) Master inverter output voltage (v_o) under disconnection of slave inverter; (b) Inductor currents (i_{L1} and i_{L2}) by AFNNISMC under disconnection of slave inverter; (c) Inductor currents (i_{L1} and i_{L2}) by ATSMC under disconnection of slave inverter; (d) Master inverter output voltage (v_o) under re-connection of slave inverter; (e) Inductor currents (i_{L1} and i_{L2}) by AFNNISMC under re-connection of slave inverter; (f) Inductor currents (i_{L1} and i_{L2}) by ATSMC under re-connection of slave inverter.

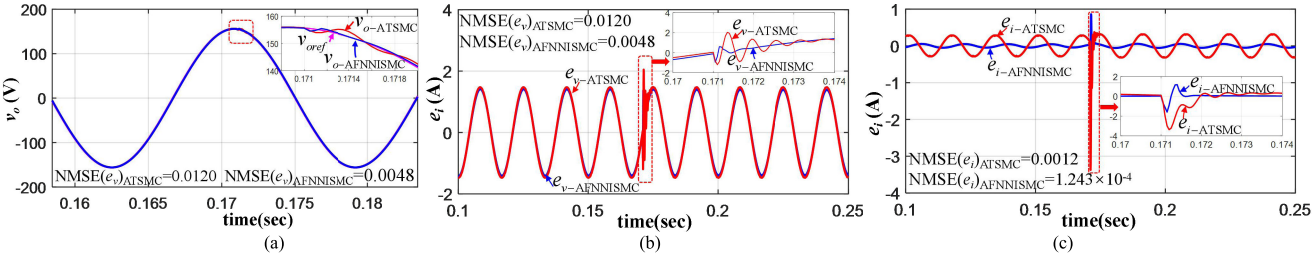

FIGURE 7. Simulated results of parallel-inverter system by AFNNISMC and ATSMC under input-voltage fluctuation of slave inverter (V_{dc1} = 200V, V_{dc2} changes from 200V to 180V): (a) Master inverter output voltage (v_o); (b) Tracking error of output voltage; (c) Sharing error of inductor current.

(0.0052 and 0.0055) by the proposed AFNNISMC. By comparing simulated results in Fig. 6, the parallel-inverter system controlled by the proposed AFNNISMC exhibits better robustness against structure uncertainties with fewer control overshoots and no chattering phenomena.

Figure 7 depicts the simulated characteristics of the output voltage regulation and current sharing of the parallel-inverter system by the designed ATSMC and the proposed AFNNISMC under the input DC voltage fluctuation of the slave inverter from 200V to 180V. The output voltage of the parallel-inverter system is depicted in Fig. 7(a) under the DC-bus voltage variation at $t = 0.171$. The voltage tracking and current sharing errors are depicted in Fig. 7(b) and 7(c), respectively. By comparing with the ATSMC framework, the proposed AFNNISMC system yields better robustness against the DC voltage variation, and provides more favorable transient performance with lower voltage tracking errors. In Fig. 7, the NMSE values for voltage tracking errors are 0.0120 by the designed ATSMC, and 0.0048 by the proposed AFNNISMC. Moreover, the NMSE values for current sharing errors are 0.0012 by the designed ATSMC and 1.243×10^{-4} by the proposed AFNNISMC.

The simulated results of the parallel-inverter system controlled by the proposed AFNNISMC and the designed ATSMC under the filter inductance deviation $\pm 10\%$ from the nominal value of 2mH in the slave inverter are depicted in Fig. 8. As can be seen from Fig. 8, the NMSE and THD values of the output voltage keep constant, and only the NMSE values of the current sharing errors have a slight increase with the increase of the inductance. It means that both the designed ATSMC and the proposed AFNNISMC strategies are less sensitive to the inductance variations.

B. EXPERIMENTAL VERIFICATION

In order to further verify the functionality of the proposed AFNNISMC strategy in practical applications, a platform with two parallel inverters is established, and its photo is depicted in Fig. 9. The DC-bus voltage of the master inverter is supplied by a DC supply (62100H-600S) manufactured by Chroma, and the voltage of the slave inverter is provided by an uncontrolled rectifier circuit with an AC voltage supplied by a voltage regulator. Moreover, full-bridge inverters are constructed with four FQA24N50F power MOSFETs, and

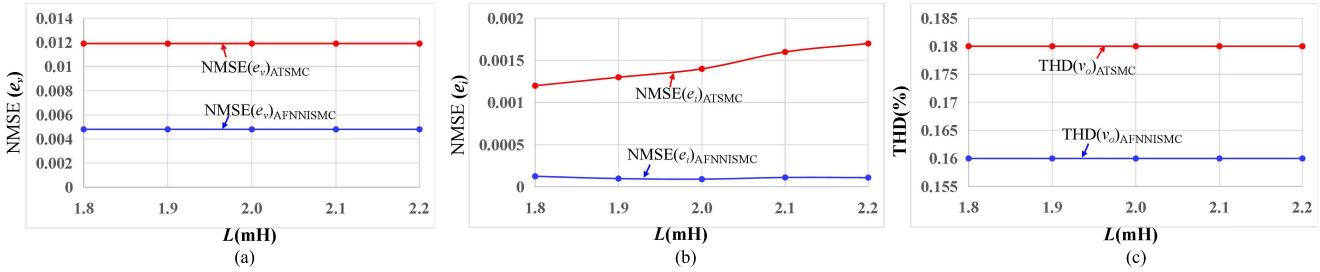

FIGURE 8. Simulated results of parallel-inverter system by AFNNISMC and ATSMC under filter inductance deviation ±10% from nominal value of 2mH: (a) NMSE value of output-voltage tracking error;(b) NMSE value of inductor-current sharing error; (c) THD value of output voltage.

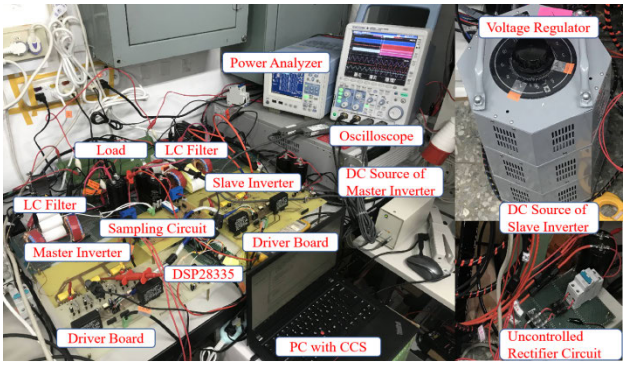

FIGURE 9. Practical photo of experimental equipment.

the corresponding driving circuit is designed based on an IC chip of TLP250.

Isolation amplifiers (AD202JN) sense terminal AC-bus voltages, and series Hall current sensors (LA 55-P) detect inductor currents inside two inverters for the feedback circuit. In addition, a TMS320F28335 series digital-signal-processor (DSP) is used to carry out a conventional proportional-integral control (PIC), the designed ATSMC, and the proposed AFNNISMC methodologies, in which the sampling frequency and switching frequency are 20kHz. The pulse-width-modulation (PWM) module in the DSP generates control signals for power switches in two inverters, and the dead times are selected as 0.5ns to avoid short-through between upper and lower MOSFETs in the same bridge. Experimental waveforms are displayed on an oscilloscope manufactured by the YOKOGAWA company, and the voltage and current probes are used to measure the output voltage and two inductor currents in the parallel-inverter system. Furthermore, the WT500 power analyzer manufactured by the YOKOGAWA company implements the harmonic analysis for the output voltage to obtain the total-harmonic-distortion (THD) value.

With the development of microelectronics and large-scale integration technologies, the performance of microprocessors has been improved unprecedentedly and the cost has been broadly reduced. Today high-performance microprocessors and DSP can be effectively used to realize advanced control schemes. A TMS320F28335 32-bit floating-point DSP with 150 MHz is used in this study.

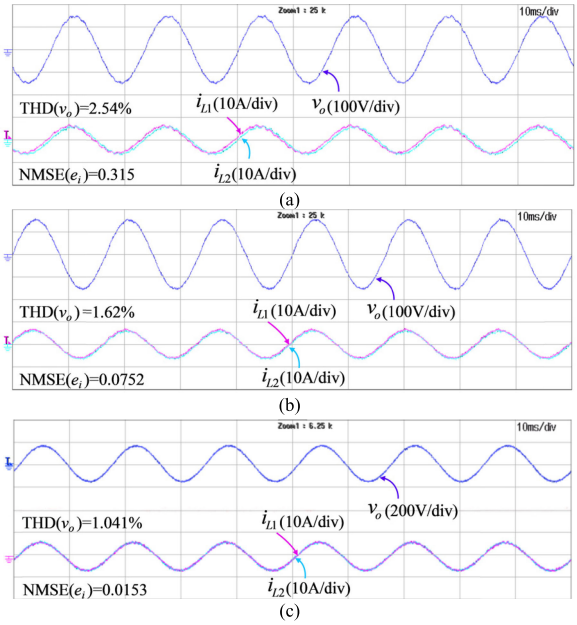

FIGURE 10. Steady-state experimental results of parallel-inverter system under resistive load: (a) PIC; (b) ATSMC; (c) AFNNISMC.

In order to implement the proposed AFNNISMC framework easily, the function approximation or look-up table method can be used to carry out Gaussian functions instead of calling math-functions codes in the code composer studio (CCS), which is helpful to decrease the execution time significantly. Moreover, some heuristics or expert knowledge can be used to pre-set the means and standard deviations of Gaussian functions for reducing the parameter training time in reality to shorten the transient training performance of the FNN. The execution time of the proposed AFNNISMC framework in the TMS320F28335 32-bit floating-point DSP with 150 MHz can be measured about 40μs, which is smaller than the sampling interval of the control loop with 0.05ms (20kHz).

In the experimentations, two inverters with the same capacity are considered, and the output voltage command of the parallel-inverter system is set as a commercial power (110V@60Hz). Moreover, the current command of the slave inverter is given by the current of the master inverter. For a fair comparison, suitable control parameters for the conventional PIC framework are selected via the Bode-plot analysis [34] to

get a control response to be similar to the one controlled by the designed ATSMC and the proposed AFNNISMC at the nominal case.

The steady-state experimental results of the parallel-inverter system controlled by the PIC, the designed ATSMC, and the proposed AFNNISMC under a resistive load ($R_l = 12.5\Omega$) are depicted in Fig. 10. The waveform of output voltage (v_o) and filter currents (i_{L1} and i_{L2}) are recorded. By observing Fig. 10(a), the THD of the output voltage by the traditional PIC is 2.54%, and the corresponding NMSE of the current sharing error between two parallel inverters is 0.315. The THD and the NMSE values recorded in Fig. 10(b) are respectively reduced to 1.62% and 0.0752 by the designed ATSMC. As for the experimental result by the proposed AFNNISMC in Fig. 10(c), the THD and NMSE values are 1.041% and 0.0153, which are lower than the ones by the conventional PIC and the designed ATSMC. Although the output voltage of the parallel-inverter system can be stably controlled to the command by all three control strategies, the proposed AFNNISMC framework yields superior responses with a lower THD in the output voltage and a lower NMSE in the current sharing.

The steady-state experimental results of the parallel-inverter system controlled by the PIC, the designed ATSMC, and the proposed AFNNISMC under a nonlinear load composed of a resistor (12.5Ω), a capacitor (1100μF) and a diode rectifier (KBPC3506P) are depicted in Fig. 11. The THD and NMSE values (3.58% and 0.416) by the PIC in Fig. 11(a) can be reduced to be 2.46% and 0.0934 by the designed ATSMC in Fig. 11(b), and to be 1.37% and 0.0283 by the proposed AFNNISMC in Fig. 11(c). It can conclude that high power quality and precise current sharing of the parallel-inverter system controlled by the proposed AFNNISMC also can be achieved under a nonlinear load.

The transient performance and the robustness against load variations by the proposed AFNNISMC are further tested here. The transient experimental results under load variations from 1kW ($R_l = 12.5\Omega$) to 500W ($R_l = 25\Omega$) are depicted in Fig. 12, and the ones under load variations from 500W ($R_l = 25\Omega$) to 1kW ($R_l = 12.5\Omega$) are depicted in Fig. 13. The NMSE values by the conventional PIC in Fig. 12(a) and Fig. 13(a) are 0.438 and 0.385, respectively. The NMSE values by the designed ATSMC in Fig. 12(b) and Fig. 13(b) are reduced to 0.0904 and 0.0837, respectively. By the proposed AFNNISMC, the NMSE values in Fig. 12(c) and Fig. 13(c) are reduced to 0.0252 and 0.0232, respectively. Moreover, the transient time by the PIC for the parallel-inverter system is about 8ms. The transient times are about 4ms and less than 1ms by the designed ATSMC and the proposed AFNNISMC, respectively. It is worth noting that the control performance of the parallel-inverter system deteriorates under the condition of a light load ($R_l = 25\Omega$) without manual re-tuning of control parameters in the PIC. The parallel-inverter system can return to stability after a short transition process with small chattering phenomena automatically by the designed ATSMC, and the chattering phenomena can be eliminated by the proposed AFNNISMC.

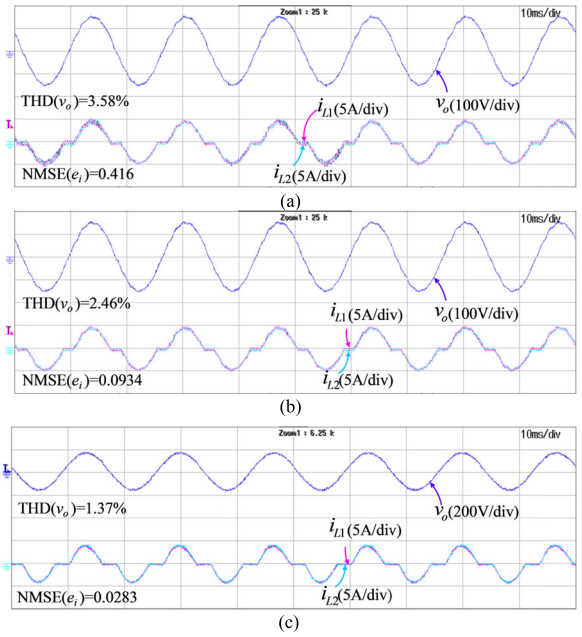

FIGURE 11. Steady-state experimental results of parallel-inverter system under nonlinear load: (a) PIC; (b) ATSMC; (c) AFNNISMC.

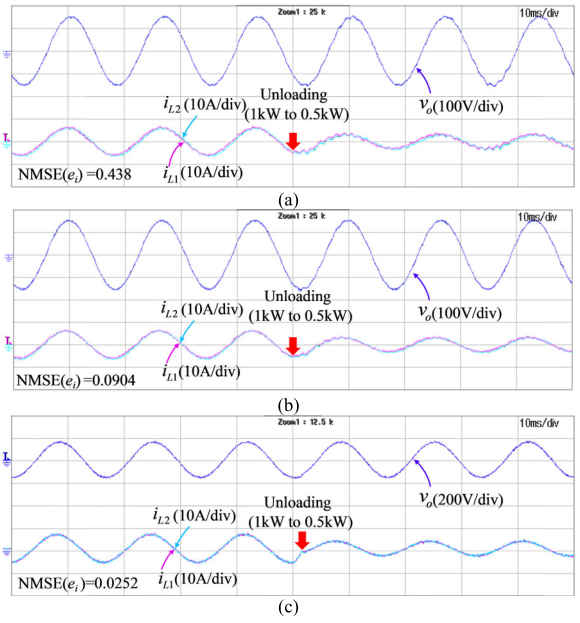

FIGURE 12. Transient experimental results of parallel-inverter system under load variations from 1kW to 500W: (a) PIC; (b) ATSMC; (c) AFNNISMC.

For a practical parallel-inverter system, the investigation of the performance with fault-inverter units is helpful and significant. The fault-inverter units should be isolated in time against accidents and re-connected to the master inverter after reparation. During the disconnection and re-connection process, the parallel-inverter system should remain workable and stability. The transient experimental results of the

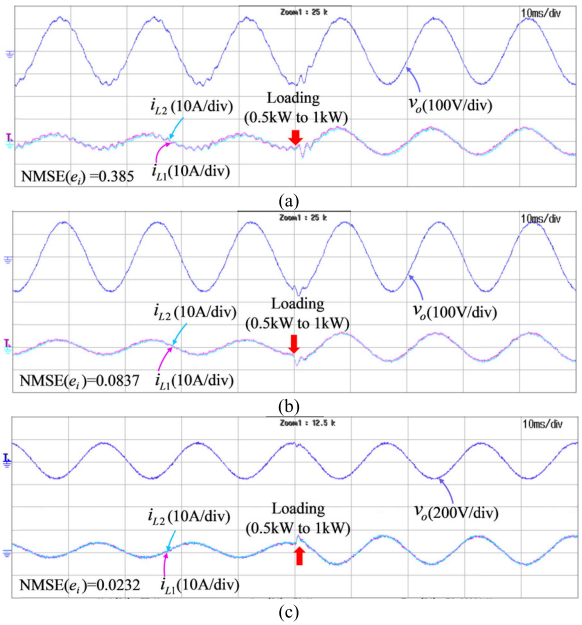

FIGURE 13. Transient experimental results of parallel-inverter system under load variations from 500W to 1kW: (a) PIC; (b) ATSMC; (c) AFNNISMC.

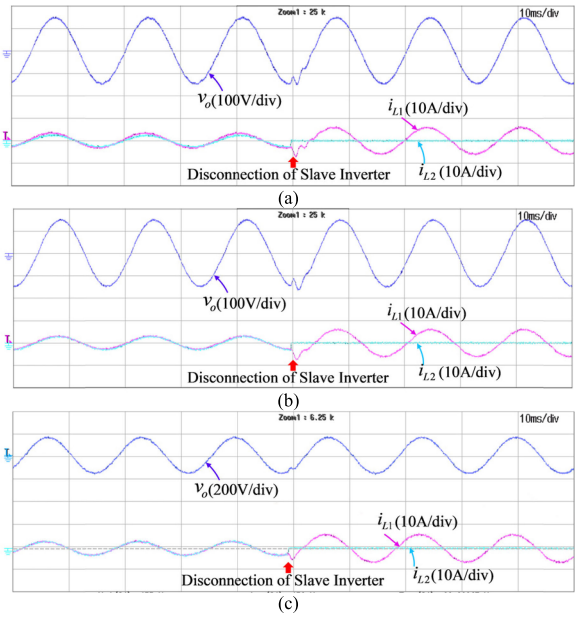

FIGURE 14. Transient experimental results of parallel-inverter systems as slave inverter disconnection: (a) PIC; (b) ATSMC; (c) AFNNISMC.

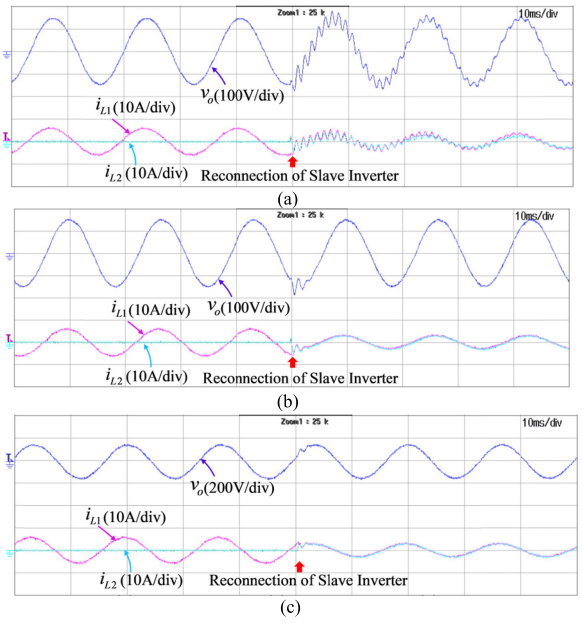

FIGURE 15. Transient experimental results of parallel-inverter system as slave inverter re-connection: (a) PIC; (b) ATSMC; (c) AFNNISMC.

parallel-inverter system under disconnection and re-connection of the slave inverter are depicted in Figs. 14 and 15, respectively. In Fig. 14, the current (i_{L2}) decreases to zero after the faulty slave inverter is disconnected from the red arrow. The master inverter can supply power to remain the output voltage as the same as the normal case, and the rated output power performs by doubling the output current of the master inverter at the front of Fig. 14. The output voltage fluctuation caused by the disconnection of the slave inverter in Fig. 14(c) is smallest by the proposed AFNNISMC by comparing with the waveforms in the transit process of the conventional PIC and the designed ATSMC in Fig. 14(a) and 14(b).

By observing Fig. 15(a), the parallel-inverter system loses its stability when the slave inverter re-connects to the master inverter after the red arrow. Because the re-connection of the slave inverter changes the impedance characteristics of the parallel-inverter system, the controller parameters in the traditional PIC are no longer suitable for the stable operation. Thus, the parallel-inverter system controlled by the PIC may be unstable if the controller parameters aren't re-tuned by manual. Favorable voltage tracking and current sharing between parallel inverters can be obtained by the designed ATSMC and the proposed AFNNISMC in Fig. 15(b) and 15(c). Despite the sudden disconnection or re-connection of the fault inverter occurred around the trough of the output voltage, the transient time is minimal and the output voltage is less influenced without chattering phenomena in the model-free AFNNISMC, which dramatically improves the availability and reliability of the parallel-inverter system.

Because DC sources in the parallel-inverter system always come from different distributed generations, DC voltages are not identical to each other due to the influence of environmental factors. The experimental result of the parallel-inverter system with different DC sources for the master and slave inverters controlled by the proposed AFNNISMC is depicted in Fig. 16. In Fig. 16, the DC voltage for the slave inverter is intentionally set to 180V from the red arrow. The THD value of the output voltage is 1.067%, and the NMSE value of the current sharing error is 0.0164. This evaluation shows that

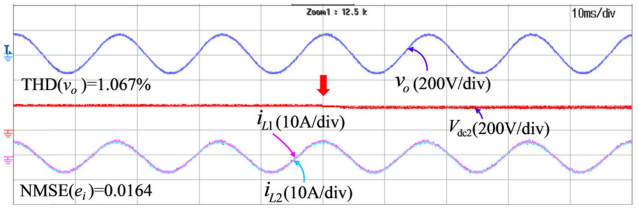

FIGURE 16. Experimental results of parallel-inverter system by AFNNISMC under different DC voltages condition ($V_{dc1} = 200$V, $V_{dc2} = 180$V).

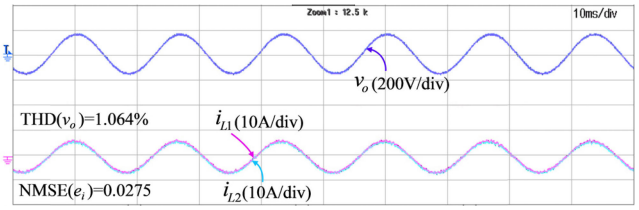

FIGURE 17. Experimental results of parallel-inverter system by AFNNISMC under asymmetrical inductances condition ($L_{f1} = 2$mH, $L_{f2} = 1.8$mH).

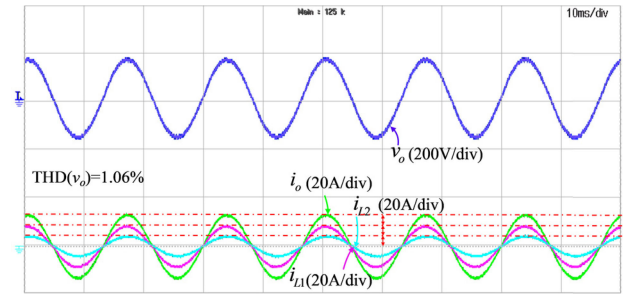

FIGURE 18. Experimental results with 2:1 current sharing ratio under resistive load.

the voltage tracking and current sharing performance by the proposed AFNNISMC is less sensitive to the difference of input DC voltages.

According to previous report in [35], the tolerance for high-quality commercial inductors is about 10%, and the filter impedance variation due to manufacturing tolerances is inevitable. Figure 17 illustrates the experimental result of the parallel-inverter system controlled by the proposed AFNNISMC under asymmetrical inductance parameters condition ($L_1 = 2$mH, $L_2 = 1.8$mH). In Fig. 17, the filter inductance of the slave inverter is intentionally decreased by –10% from the nominal value of 2mH. It can be seen that the THD value of the output voltage is 1.064%, and the NMSE value of the current sharing error is 0.0275 under the condition of asymmetrical inductances. As a result, it confirms that the quality of the output voltage and the current-sharing error introduced by the filter impedance deviation can be removed in the proposed AFNNISMC strategy.

Figure 18 illustrates the experimental results of the parallel-inverter system with a 2:1 current sharing ratio under the resistive load to further confirm the effectiveness of the proposed AFNNISMC. In Fig. 18, the command of the inductor current in the slave inverter is set as $i_{L2}^{ref} = 0.5 \times i_{L1}$. As can be seen from Fig. 18, the proportional current sharing between the master and slave inverters can be accurately performed to be 2:1, and the output voltage also can be regulated to the command with a low THD value (1.06%).

VI. CONCLUSION

In this study, a model-free adaptive fuzzy-neural-network-imitating sliding-mode control (AFNNISMC) with a master-slave current sharing strategy is proposed for a parallel-inverter system in an islanded micro-grid (MG). First, the entire dynamic model is analyzed for the controller design and the system-level stability analysis by viewing parallel inverters containing a master inverter and n-1 slave inverters as a whole. Then, a total sliding-surface vector composed of the elements of the voltage-tracking error and the current-sharing error is designed. Moreover, an adaptive total sliding-mode control (ATSMC) law for the parallel-inverter system with global robustness can be obtained by combining an adaptive observer for the control gain of the curbing controller into the total sliding-mode control (TSMC). In addition, the elements of the total sliding-surface vector are taken as the inputs of the designed fuzzy neural network (FNN) to imitate the TSMC law. Furthermore, self-tuning laws of network parameters in the AFNNISMC are derived from system stability analyses. The function of the proposed AFNNISMC framework is not affected by the disconnection and re-connection of partial slave inverters, and the system stability also can be ensured under the occurrence of structure uncertainties. Thus, the robustness of the voltage tracking and current sharing can be obtained both under the occurrence of parameter variations and structure uncertainties. By comparing a conventional proportional-integral control (PIC), the designed ATSMC, and the proposed AFNNISMC frameworks at different operating conditions to be implemented on the same microprocessor, it is proved that the proposed AFNNISMC system is feasible and effective, and the corresponding performance analytic results are summarized in Table 3.

As can be seen from Table 3, the total-harmonic-distortion (THD) value of the voltage tracking, and the normalized-mean-square-error (NMSE) of the current sharing in the designed ATSMC are smaller than those controlled by the conventional PIC; but larger than those controlled by the proposed AFNNISMC under the same operational conditions. Moreover, the designed ATSMC and the proposed AFNNISMC both have good robustness under system uncertainties. However, the number of poles and zeros in the parallel-inverter system may be changed due to the disconnection and re-connection of someone slave inverters. If control parameters in the conventional PIC scheme are not manually adjusted, the system will be unstable under the occurrence of structure change. Even though the adaptive ability is introduced into the ATSMC for identifying system uncertainties to improve the transient response performance, the detailed system dynamic is always required in this

TABLE 3. Performance comparisons of different control methods.

Performance	Control Method		PI	ATSMC	AFNNISMC
Steady –state performance	Resistive load	THD(v_o)	2.54%	1.62%	1.041%
		NMSE(e_i)	0.315	0.0752	0.0153
	Nonlinear load	THD(v_o)	3.58%	2.46%	1.37%
		NMSE(e_i)	0.416	0.0934	0.0283
Dynamic Performance	Power variations from 500W to 1kW	NMSE(e_i)	0.385	0.0837	0.0232
		Control chattering	High	Low	None
	Power variations from 1kW to 500W	NMSE(e_i)	0.438	0.0904	0.0252
		Control chattering	High	Low	None
	Disconnection of slave inverter	Stability	Yes	Yes	Yes
		Control chattering	High	Low	None
	Re-connection of slave inverter	Stability	No	Yes	Yes
		Control chattering	High	Low	None
Requirement of system information			Low	High	None
Learning and reasoning ability			None	None	On-line learning and reasoning
Computation time			Low	Low	High

model-based ATSMC framework such that the chattering phenomena are inevitable.

The proposed AFNNISMC strategy possesses good static performance and strong robustness against system uncertainties with a smaller overshoot and a faster response. Moreover, the chattering phenomena caused by the sign function in the ATSMC can be eliminated, and the implementation of the proposed AFNNISMC without the requirement of complex mathematical dynamic models. Network parameters in the proposed AFNNISMC can be roughly initialized, and then optimized by online learning laws. In addition, three control methodologies including PIC, ATSMC and AFNNISMC are implemented on the same TMS320F28335 series DSP with the sampling time of 0.05ms. Due to the development of microprocessors in recent years, the proposed AFNNISMC algorithm indeed can be executed completely within a sampling interval. According to performance comparisons in Table 3, the proposed AFNNISMC with online learning ability is worthy to be developed in the parallel-inverter system, even it requires more computation time.

The proposed model-free AFNNISMC scheme can effectively improve the robustness of the parallel-inverter system against system uncertainties without additional compensation controllers. However, a high computational cost may be concerned, especially when the number of paralleled inverters increases. In the future research, the method to reduce the computational complexity can be further developed. Moreover, the FNN structure in the proposed AFNNISMC system remains unchanged with the disconnection or re-connection of partial slave inverters to guarantee the robustness against structure uncertainties. But, the parameters with respect to slave inverters are still updated online even though partial slave inverters disconnect from the parallel-inverter system, which will increase the computation burden. It is worthy to study a variable-structure neural network or adaptive-feature-selection-based schemes in the control of a parallel-inverter system. In addition, in order to obtain the better imitating performance, a recurrent framework involving feedback connections can be adopted to enhance the generalization property of FNN in the future research.

APPENDIX

By taking the derivative of (30) with respect to time, one can obtain

$$\dot{V}_{\text{AFNNISMC}}(\boldsymbol{s}, \tilde{\boldsymbol{w}}_{ts}, \tilde{\boldsymbol{m}}, \tilde{\boldsymbol{c}}) = \boldsymbol{s}^T \dot{\boldsymbol{s}} - \frac{\dot{\hat{\boldsymbol{w}}}_{ts}^T \tilde{\boldsymbol{w}}_{ts}}{\eta_{ws}} - \frac{\dot{\hat{\boldsymbol{m}}}^T \tilde{\boldsymbol{m}}}{\eta_{ms}} - \frac{\dot{\hat{\boldsymbol{c}}}^T \tilde{\boldsymbol{c}}}{\eta_{cs}} \tag{A1}$$

To rewrite (23) by replacing $\boldsymbol{u}_{\text{TSMC}}$ with (10) and $\tilde{\boldsymbol{u}}_s$ with (26), the proposed adaptive fuzzy-neural-network-imitating sliding-mode control (AFNNISMC) law can be formulated as follows:

$$\begin{aligned}\hat{\boldsymbol{u}}_{\text{AFNNISMC}} &= \boldsymbol{u}_{\text{TSMC}} - \tilde{\boldsymbol{u}}_s \\ &= [-\mathbf{B}_{pn}^{-1}(\boldsymbol{A}_{pn}\boldsymbol{x} + \boldsymbol{C}_{pn}\boldsymbol{z} - \dot{\boldsymbol{x}}_d) + \frac{\partial f}{\partial \boldsymbol{e}^T} J\boldsymbol{e}] + \mathbf{B}_{pn}^{-1}[\rho \text{sgn}(\boldsymbol{s}) \\ &\quad + \mathbf{K}_s \boldsymbol{s}] - (\mathbf{Y}_{ws}\tilde{\boldsymbol{w}}_{ts} + \mathbf{U}_{ls}\boldsymbol{l}_{ms}\tilde{\boldsymbol{m}} + \mathbf{U}_{ls}\boldsymbol{l}_{cs}\tilde{\boldsymbol{c}} + \boldsymbol{y}_s')\end{aligned} \tag{A2}$$

By substituting $\hat{\boldsymbol{u}}_{\text{AFNNISMC}}$ in (A2) into the control effort ($\boldsymbol{u}$) in (4), the differential of the total sliding-surface vector in (9) can be rewritten as

$$\begin{aligned}\dot{\boldsymbol{s}} = &-\mathbf{B}_{pn}^{-1}[\rho \text{sgn}(\boldsymbol{s}) + \mathbf{K}_s \boldsymbol{s} + \boldsymbol{\psi}] \\ &+(\mathbf{Y}_{ws}\tilde{\boldsymbol{w}}_{ts}^T + \mathbf{U}_{ls}\boldsymbol{l}_{ms}\tilde{\boldsymbol{m}} + \mathbf{U}_{ls}\boldsymbol{l}_{cs}\tilde{\boldsymbol{c}} + \boldsymbol{y}_s')\end{aligned} \tag{A3}$$

By substituting (A3) into (A1), one can obtain

$$\begin{aligned}&\dot{V}_{\text{AFNNISMC}} \\ &= \boldsymbol{s}^T \mathbf{B}_{pn}^{-1}[-\rho \text{sgn}(\boldsymbol{s}) - \mathbf{K}_s \boldsymbol{s} - \boldsymbol{\psi}] \\ &\quad +\boldsymbol{s}^T(\mathbf{Y}_{ws}\tilde{\boldsymbol{w}}_{ts} + \mathbf{U}_{ls}\boldsymbol{l}_{ms}\tilde{\boldsymbol{m}} + \mathbf{U}_{ls}\boldsymbol{l}_{cs}\tilde{\boldsymbol{c}} + \boldsymbol{y}_s') \\ &\quad -\frac{\dot{\hat{\boldsymbol{w}}}_{ts}^T \tilde{\boldsymbol{w}}_{ts}}{\eta_{ws}} - \frac{\dot{\hat{\boldsymbol{m}}}^T \tilde{\boldsymbol{m}}}{\eta_{ms}} - \frac{\dot{\hat{\boldsymbol{c}}}^T \tilde{\boldsymbol{c}}}{\eta_{cs}} \\ &= \boldsymbol{s}^T \mathbf{B}_{pn}^{-1}[-\rho \text{sgn}(\boldsymbol{s}) - \mathbf{K}_s \boldsymbol{s} - \boldsymbol{\psi} - \mathbf{B}_{pn}\boldsymbol{y}_s'] \\ &\quad +(\boldsymbol{s}^T \mathbf{Y}_{ws}\tilde{\boldsymbol{w}}_{ts} - \frac{\dot{\hat{\boldsymbol{w}}}_{ts}^T \tilde{\boldsymbol{w}}_{ts}}{\eta_{ws}}) + (\boldsymbol{s}^T \mathbf{U}_{ls}\boldsymbol{l}_{ms}\tilde{\boldsymbol{m}} - \frac{\dot{\hat{\boldsymbol{m}}}^T \tilde{\boldsymbol{m}}}{\eta_{ms}}) \\ &\quad +(\boldsymbol{s}^T \mathbf{U}_{ls}\boldsymbol{l}_{cs}\tilde{\boldsymbol{c}} - \frac{\dot{\hat{\boldsymbol{c}}}^T \tilde{\boldsymbol{c}}}{\eta_{cs}}) \\ &= \boldsymbol{s}^T \mathbf{B}_{pn}^{-1}[-\rho \text{sgn}(\boldsymbol{s}) - \mathbf{K}_s \boldsymbol{s} - \boldsymbol{\psi} - \mathbf{B}_{pn}\boldsymbol{y}_s'] \\ &\quad +V_{ws} + V_{ms} + V_{cs}\end{aligned} \tag{A4}$$

where $V_{ws} = \boldsymbol{s}^T\mathbf{Y}_{ws}\tilde{\boldsymbol{w}}_{ts} - \dot{\hat{\boldsymbol{w}}}_{ts}^T\tilde{\boldsymbol{w}}_{ts}/\eta_{ws}$, $V_{ms} = \boldsymbol{s}^T\mathbf{U}_{ls}\boldsymbol{l}_{ms}\tilde{\boldsymbol{m}} - \frac{\dot{\hat{\boldsymbol{m}}}^T\tilde{\boldsymbol{m}}}{\eta_{ms}}$ and $V_{cs} = \boldsymbol{s}^T\mathbf{U}_{ls}\boldsymbol{l}_{cs}\tilde{\boldsymbol{c}} - \frac{\dot{\hat{\boldsymbol{c}}}^T\tilde{\boldsymbol{c}}}{\eta_{cs}}$.

If the adaptation law for the weights in the proposed AFNNISMC is designed as (27), V_{ws} can be represented as

By (27a):

$$\begin{aligned} V_{ws} &= \boldsymbol{s}^T\mathbf{Y}_{ws}\tilde{\boldsymbol{w}}_{ts} - \dot{\hat{\boldsymbol{w}}}_{ts}^T\tilde{\boldsymbol{w}}_{ts}/\eta_{ws} \\ &= \boldsymbol{s}^T\mathbf{Y}_{ws}\tilde{\boldsymbol{w}}_{ts} - (\eta_{ws}\boldsymbol{s}^T\mathbf{Y}_{ws})\tilde{\boldsymbol{w}}_{ts}/\eta_{ws} \\ &= \boldsymbol{s}^T\mathbf{Y}_{ws}\tilde{\boldsymbol{w}}_{ts} - \boldsymbol{s}^T\mathbf{Y}_{ws}\tilde{\boldsymbol{w}}_{ts} = 0 \end{aligned} \tag{A5}$$

By (27b):

$$\begin{aligned} V_{ws} &= \boldsymbol{s}^T\mathbf{Y}_{ws}\tilde{\boldsymbol{w}}_{ts} - \dot{\hat{\boldsymbol{w}}}_{ts}^T\tilde{\boldsymbol{w}}_{ts}/\eta_{ws} \\ &= \boldsymbol{s}^T\mathbf{Y}_{ws}\tilde{\boldsymbol{w}}_{ts}^T - [\boldsymbol{s}^T\mathbf{Y}_{ws} - (\boldsymbol{s}^T\mathbf{Y}_{ws}\hat{\boldsymbol{w}}_{ts}\hat{\boldsymbol{w}}_{ts}^T/\left\|\hat{\boldsymbol{w}}_{ts}\right\|^2)]\tilde{\boldsymbol{w}}_{ts} \\ &= \boldsymbol{s}^T\mathbf{Y}_{ws}\hat{\boldsymbol{w}}_{ts}(\hat{\boldsymbol{w}}_{ts}^T\tilde{\boldsymbol{w}}_{ts}/\left\|\hat{\boldsymbol{w}}_{ts}\right\|^2) \end{aligned} \tag{A6}$$

If the conditions of $\left\|\hat{\boldsymbol{w}}_{ts}\right\| = b_{ws}$ and $\boldsymbol{s}^T\mathbf{Y}_{ws}\hat{\boldsymbol{w}}_{ts} > 0$ are satisfied, the results of $\hat{\boldsymbol{w}}_{ts}^T\tilde{\boldsymbol{w}}_{ts} = \hat{\boldsymbol{w}}_{ts}^T(\boldsymbol{w}_{ts}^* - \hat{\boldsymbol{w}}_{ts}) = \frac{1}{2}(\left\|\boldsymbol{w}_{ts}^*\right\|^2 - \left\|\hat{\boldsymbol{w}}_{ts}\right\|^2 - \|\tilde{\boldsymbol{w}}_{ts}\|^2) < 0$ holds. Moreover, the fact of $V_{ws} < 0$ can be obtained according to $\left\|\boldsymbol{w}_{ts}^*\right\| < b_{ws} = \left\|\hat{\boldsymbol{w}}_{ts}\right\|$ and (A7). From the analyses in (A6) and (A7), one can conclude that $V_{ws} \leq 0$. Similarly, it turns out that $V_{ms} \leq 0$ and $V_{cs} \leq 0$ also hold. Then, (A4) can be represented

$$\begin{aligned} &\dot{V}_{\text{AFNNISMC}} \\ &= \boldsymbol{s}^T\mathbf{B}_{pn}^{-1}[-\rho\text{sgn}(\boldsymbol{s}) - \mathbf{K}_s\boldsymbol{s} - \boldsymbol{\psi} + \mathbf{B}_{pn}\boldsymbol{y}_s'] \\ &\quad + V_{ws} + V_{ms} + V_{cs} \\ &\leq -\boldsymbol{s}^T\mathbf{B}_{pn}^{-1}\mathbf{K}_s\boldsymbol{s} - \boldsymbol{s}^T\mathbf{B}_{pn}^{-1}(\boldsymbol{\psi} - \mathbf{B}_{pn}\boldsymbol{y}_s') \\ &\quad -\boldsymbol{s}^T\mathbf{B}_{pn}^{-1}\rho\text{sgn}(\boldsymbol{s}) \\ &\leq -\boldsymbol{s}^T\mathbf{B}_{pn}^{-1}\mathbf{K}_s\boldsymbol{s} - \left\|\boldsymbol{s}^T\mathbf{B}_{pn}^{-1}\right\|_1[\rho - \left\|\mathbf{B}_{pn}\boldsymbol{y}_s' - \boldsymbol{\psi}\right\|_1] \end{aligned} \tag{A7}$$

If the gain condition of $\rho > \left\|\mathbf{B}_{pn}\boldsymbol{y}_s' - \boldsymbol{\psi}\right\|_1$ is designed, the result of $\dot{V}_{\text{AFNNISMC}} \leq -\boldsymbol{s}^T\mathbf{B}_{pn}^{-1}\mathbf{K}_s\boldsymbol{s} \leq 0$ can be satisfied.

REFERENCES

[1] D. Wu, F. Tang, T. Dragicevic, J. C. Vasquez, and J. M. Guerrero, "A control architecture to coordinate renewable energy sources and energy storage systems in islanded microgrids," *IEEE Trans. Smart Grid*, vol. 6, no. 3, pp. 1156–1166, May 2015.

[2] S. Kakran and S. Chanana, "Smart operations of smart grids integrated with distributed generation: A review," *Renew. Sustain. Energy Rev.*, vol. 81, pp. 524–535, Jan. 2018.

[3] S. Rahmani, A. Rezaei-Zare, M. Rezaei-Zare, and A. Hooshyar, "Voltage and frequency recovery in an islanded inverter-based microgrid considering load type and power factor," *IEEE Trans. Smart Grid*, vol. 10, no. 6, pp. 6237–6247, Nov. 2019.

[4] A. Mortezaei, M. G. Simões, M. Savaghebi, J. M. Guerrero, and A. Al-Durra, "Cooperative control of multi-master-slave islanded microgrid with power quality enhancement based on conservative power theory," *IEEE Trans. Smart Grid*, vol. 9, no. 4, pp. 2964–2975, Jul. 2018.

[5] S. Yazdani, M. Ferdowsi, M. Davari, and P. Shamsi, "Advanced current-limiting and power-sharing control in a PV-based grid-forming inverter under unbalanced grid conditions," *IEEE J. Emerg. Sel. Topics Power Electron.*, vol. 8, no. 2, pp. 1084–1096, Jun. 2020.

[6] P. Jain, V. Agarwal, and B. P. Muni, "Hybrid phase locked loop for controlling master-slave configured centralized inverters in large solar photovoltaic power plants," *IEEE Trans. Ind. Appl.*, vol. 54, no. 4, pp. 3566–3574, Jul. 2018.

[7] X. Meng, Z. Liu, H. Zheng, and J. Liu, "A universal controller under different operating states for parallel inverters with seamless transfer capability," *IEEE Trans. Power Electron.*, vol. 35, no. 9, pp. 9794–9812, Sep. 2020.

[8] B. Zhao, C. Wang, and X. Zhang, "A survey of suitable energy storage for island stand-alone microgrid and commercial operation mode," *Autom. Electr. Power Syst.*, vol. 37, no. 4, pp. 21–27, Apr. 2013.

[9] S. Tolani and P. Sensarma, "An instantaneous average current sharing scheme for parallel UPS modules," *IEEE Trans. Ind. Electron.*, vol. 64, no. 12, pp. 9210–9220, Dec. 2017.

[10] J. Chen, S. Hou, and J. Chen, "Seamless mode transfer control for master-slave microgrid," *IET Power Electron.*, vol. 12, no. 12, pp. 3158–3165, Oct. 2019.

[11] M. B. Delghavi and A. Yazdani, "Sliding-mode control of AC voltages and currents of dispatchable distributed energy resources in master-slave-organized inverter-based microgrids," *IEEE Trans. Smart Grid*, vol. 10, no. 1, pp. 980–991, Jan. 2019.

[12] Q.-C. Zhong, Y. Wang, and B. Ren, "UDE-based robust droop control of inverters in parallel operation," *IEEE Trans. Ind. Electron.*, vol. 64, no. 9, pp. 7552–7562, Sep. 2017.

[13] X. Huang, K. Wang, J. Qiu, L. Hang, G. Li, and X. Wang, "Decentralized control of multi-parallel grid-forming DGs in islanded microgrids for enhanced transient performance," *IEEE Access*, vol. 7, pp. 17958–17968, Feb. 2019.

[14] C. Zhang, J. M. Guerrero, J. C. Vasquez, and E. A. A. Coelho, "Control architecture for parallel-connected inverters in uninterruptible power systems," *IEEE Trans. Power Electron.*, vol. 31, no. 7, pp. 5176–5188, Jul. 2016.

[15] Y. Wu, J. M. Guerrero, and Y. Wu, "Distributed coordination control for suppressing circulating current in parallel inverters of islanded microgrid," *IET Gener., Transmiss. Distrib.*, vol. 13, no. 7, pp. 968–975, Apr. 2019.

[16] M. A. Setiawan, F. Shahnia, S. Rajakaruna, and A. Ghosh, "ZigBee-based communication system for data transfer within future microgrids," *IEEE Trans. Smart Grid*, vol. 6, no. 5, pp. 2343–2355, Sep. 2015.

[17] H.-J. Choi and J.-H. Jung, "Enhanced power line communication strategy for DC microgrids using switching frequency modulation of power converters," *IEEE Trans. Power Electron.*, vol. 32, no. 6, pp. 4140–4144, Jun. 2017.

[18] D. Li and C. N. M. Ho, "Master-slave control of parallel-operated interfacing inverters based on wireless digital communication," in *Proc. IEEE Energy Convers. Congr. Expo.*, Portland, OR, USA, Sep. 2018, pp. 1466–1472.

[19] D. Li and C. N. M. Ho, "A delay-tolerable master-slave current-sharing control scheme for parallel-operated interfacing inverters with low-bandwidth communication," *IEEE Trans. Ind. Appl.*, vol. 56, no. 2, pp. 1575–1586, Mar. 2020.

[20] K.-H. Tan, F.-J. Lin, C.-M. Shih, and C.-N. Kuo, "Intelligent control of microgrid with virtual inertia using recurrent probabilistic wavelet fuzzy neural network," *IEEE Trans. Power Electron.*, vol. 35, no. 7, pp. 7451–7464, Jul. 2020.

[21] X. Li, L. Guo, and C. Wang, "Stability Analysis in a master-slave control based microgrid," *Trans. China Electrotech. Soc.*, vol. 29, no. 2, pp. 24–34, Feb. 2014.

[22] X. Sun, H. Ma, L. Jia, and X. Li, "A robust control strategy for eliminating the structure disturbance of islanding microgrid," *Trans. China Electrotech. Soc.*, vol. 35, no. 11, pp. 149–160, Jun. 2020.

[23] Z. Liu, J. Liu, X. Hou, Q. Dou, D. Xue, and T. Liu, "Output impedance modeling and stability prediction of three-phase paralleled inverters with master-slave sharing scheme based on terminal characteristics of individual inverters," *IEEE Trans. Power Electron.*, vol. 31, no. 7, pp. 5306–5320, Jul. 2016.

[24] H. Li, P. Shi, and D. Yao, "Adaptive sliding-mode control of Markov jump nonlinear systems with actuator faults," *IEEE Trans. Autom. Control*, vol. 62, no. 4, pp. 1933–1939, Apr. 2017.

[25] G. Zhong, Z. Shao, H. Deng, and J. Ren, "Precise position synchronous control for multi-axis servo systems," *IEEE Trans. Ind. Electron.*, vol. 64, no. 5, pp. 3707–3717, May 2017.

[26] I. U. Haq, Q. Khan, I. Khan, R. Akmeliawati, K. S. Nisar, and I. Khan, "Maximum power extraction strategy for variable speed wind turbine system via neuro-adaptive generalized global sliding mode controller," *IEEE Access*, vol. 8, pp. 128536–128547, Jan. 2020.

[27] C. T. Lin and C. S. G. Lee, *Neural Fuzzy Systems*. Upper Saddle River, NJ, USA: Prentice-Hall, 1996.
[28] S. Hou, J. Fei, C. Chen, and Y. Chu, "Finite-time adaptive fuzzy-neural-network control of active power filter," *IEEE Trans. Power Electron.*, vol. 34, no. 10, pp. 10298–10313, Oct. 2019.
[29] Y. Chu, J. Fei, and S. Hou, "Adaptive global sliding-mode control for dynamic systems using double hidden layer recurrent neural network structure," *IEEE Trans. Neural Netw. Learn. Syst.*, vol. 31, no. 4, pp. 1297–1309, Apr. 2020.
[30] S. Hou and J. Fei, "A self-organizing global sliding mode control and its application to active power filter," *IEEE Trans. Power Electron.*, vol. 35, no. 7, pp. 7640–7652, Jul. 2020.
[31] S. Hou, Y. Chu, and J. Fei, "Intelligent global sliding mode control using recurrent feature selection neural network for active power filter," *IEEE Trans. Ind. Electron.*, early access, Jun. 12, 2020, doi: 10.1109/TIE.2020.3000098.
[32] S. Hou, Y. Chu, and J. Fei, "Adaptive type-2 fuzzy neural network inherited terminal sliding mode control for power quality improvement," *IEEE Trans. Ind. Informat.*, early access, Jan. 6, 2021, doi: 10.1109/TII.2021.3049643.
[33] K. J. Astrom and B. Wittenmark, *Adaptive Control*. New York, NY, USA: Addison-Wesley, 1995.
[34] R.-J. Wai and Y. Yang, "Design of backstepping direct power control for three-phase PWM rectifier," *IEEE Trans. Ind. Appl.*, vol. 55, no. 3, pp. 3160–3173, May 2019.
[35] Y. Li, R. Mai, L. Lu, and Z. He, "Active and reactive currents decomposition-based control of angle and magnitude of current for a parallel multiinverter IPT system," *IEEE Trans. Power Electron.*, vol. 32, no. 2, pp. 1602–1614, Feb. 2017.

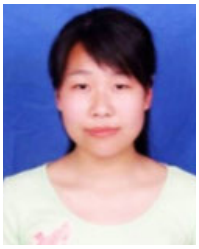

YAN YANG was born in Jiangsu, China, in 1984. She received the M.S. degree from the China University of Mining and Technology, China, in 2009. She is currently pursuing the Ph.D. degree with the Department of Electrical Engineering and Computer Science, National Taiwan University of Science and Technology, Taipei, Taiwan. She is currently a Lecturer with the Department of Automation, Huaiyin Institute of Technology, China. Her research interests include smart micro-grids and non-linear control of power converter.

RONG-JONG WAI (Senior Member, IEEE) was born in Tainan, Taiwan, in 1974. He received the B.S. degree in electrical engineering and the Ph.D. degree in electronic engineering from Chung Yuan Christian University, Chung Li, Taiwan, in 1996 and 1999, respectively.

From August 1998 to July 2015, he was with Yuan Ze University, Chung Li, where he was the Dean of General Affairs from August 2008 to July 2013, and the Chairman with the Department of Electrical Engineering from August 2014 to July 2015. Since August 2015, he has been with National Taiwan University of Science and Technology, Taipei, Taiwan, where he was the Dean of General Affairs from August 2018 to January 2021. He is currently a Distinguished Professor, and the Director of the Energy Technology and Mechatronics Laboratory. He is also a Fellow of the Institution of Engineering and Technology, U.K. and a Senior Member of the Institute of Electrical and Electronics Engineers, USA. The outstanding achievement of his research is for contributions to real-time intelligent control in practical applications and high-efficiency power converters in energy technology. He has authored more than 170 conference papers, over 190 international journal articles, and 59 inventive patents. His research interests include power electronics, motor servo drives, mechatronics, energy technology, and control theory applications.

Dr. Wai received the Excellent Research Award in 2000; the Wu Ta-You Medal and Young Researcher Award from the National Science Council, Taiwan, in 2003; the Outstanding Research Award from the Yuan Ze University, Taiwan, in 2003 and 2007; the Excellent Young Electrical Engineering Award and the Outstanding Electrical Engineering Professor Award from the Chinese Electrical Engineering Society, Taiwan, in 2004 and 2010; the Outstanding Professor Award from the Far Eastern Y. Z. Hsu-Science and Technology Memorial Foundation, Taiwan, in 2004 and 2008; the International Professional of the Year Award from the International Biographical Centre, U.K., in 2005; the Young Automatic Control Engineering Award from the Chinese Automatic Control Society, Taiwan, in 2005; the Yuan-Ze Chair Professor Award from the Far Eastern Y. Z. Hsu-Science and Technology Memorial Foundation, Taiwan, in 2007, 2010, and 2013; the Electric Category-Invent Silver Medal Award in 2007; the Electronic Category-Invent Gold and Silver Medal Awards in 2008; the Environmental Protection Category-Invent Gold Medal Award in 2008; the Most Environmental Friendly Award in 2008; the University Industrial Economic Contribution Award from the Ministry of Economic Affairs, Taiwan, in 2010; the Ten Outstanding Young Award from the Ten Outstanding Young Person's Foundation, Taiwan, in 2012; the Taiwan Top 100 MVP Managers Award from MANAGER today magazine, Taiwan, in 2012; the Power Category-Invent Bronze Medal Award in 2012; the Outstanding Engineering Professor Award from the Chinese Institute of Engineers, Taiwan, in 2013; the Green Technology Category-Scientific Paper Award from the Far Eastern Y. Z. Hsu-Science and Technology Memorial Foundation, Taiwan, in 2014; the Scopus Young Researcher Lead Award-Computer Science from Taiwan Elsevier in 2014; the Electronic Category-Invent Gold and Silver Medal Awards from the International Invention Show and Technomart, Taipei, Taiwan, in 2015; the Outstanding Research Award from the National Taiwan University of Science and Technology, Taiwan, in 2016, 2018, and 2020; the Most Cited Researchers Award in 2016 (Field: Electrical & Electronics Engineering), and the World's Top 2% of Scientists (Rank 17th, Field: Electrical & Electronics Engineering) in 2020.